Scientific Reports

https://doi.org/10.1038/s41598-026-53702-1

Article in Press

Optimizing the mechanical performance of adobe bricks reinforced with *Vicia faba* plant waste and derived biochar using ANN and RSM

Received: 22 March 2026

Accepted: 13 May 2026

Published online: 18 May 2026

Cite this article as: Frioui N., Boumaaza M., Belaadi A. *et al.* Optimizing the mechanical performance of adobe bricks reinforced with *Vicia faba* plant waste and derived biochar using ANN and RSM. *Sci Rep* (2026). https://doi.org/10.1038/s41598-026-53702-1

Nadia Frioui, Messaouda Boumaaza, Ahmed Belaadi, Mahmood M. S. Abdullah, Djamel Ghernaout, Amar Al-Khawlani & Herbert Mukalazi

We are providing an unedited version of this manuscript to give early access to its findings. Before final publication, the manuscript will undergo further editing. Please note there may be errors present which affect the content, and all legal disclaimers apply.

If this paper is publishing under a Transparent Peer Review model then Peer Review reports will publish with the final article.

ARTICLE IN PRESS

© The Author(s) 2026. **Open Access** This article is licensed under a Creative Commons Attribution-NonCommercial-NoDerivatives 4.0 International License, which permits any non-commercial use, sharing, distribution and reproduction in any medium or format, as long as you give appropriate credit to the original author(s) and the source, provide a link to the Creative Commons licence, and indicate if you modified the licensed material. You do not have permission under this licence to share adapted material derived from this article or parts of it. The images or other third party material in this article are included in the article's Creative Commons licence, unless indicated otherwise in a credit line to the material. If material is not included in the article's Creative Commons licence and your intended use is not permitted by statutory regulation or exceeds the permitted use, you will need to obtain permission directly from the copyright holder. To view a copy of this licence, visit http://creativecommons.org/licenses/by-nc-nd/4.0/.

ARTICLE IN PRESS

Optimizing the Mechanical Performance of Adobe Bricks Reinforced with *Vicia faba* Plant Waste and Derived Biochar Using ANN and RSM

Nadia Frioui[1], Messaouda Boumaaza[2], Ahmed Belaadi[3*], Mahmood M. S. Abdullah[4], Djamel Ghernaout[5], Amar Al-Khawlani[6] and Herbert Mukalazi[7*]

1 Department of Mechanical Engineering, Faculty of Science and Technology, University 8 Mai 1945 Guelma, 401, Guelma, BP 24000, Algeria.
2 Laboratory of Civil Engineering and Hydraulics (LGCH), University 8 Mai 1945 Guelma, 401, Guelma, BP 24000, Algeria.
3 Department of Mechanical Engineering, Faculty of Technology, University 20 Août 1955-Skikda, El-Hadaiek, Skikda, Algeria.
4 Department of Chemistry, College of Science, King Saud University, PO Box 2455, Riyadh 11451, Saudi Arabia.
5 Chemical Engineering Department, College of Engineering, University of Ha'il, PO Box 2440, Ha'il 81441, Saudi Arabia.
6 Southeast University, Jiangsu Optoelectronic Functional Materials and Engineering Research Centre, School of Chemistry and Chemical Engineering, Nanjing, China.
7 Department of Mathematics and Statistics, Kyambogo University, Kampala, Uganda

Corresponding author: A. Belaadi: ahmedbelaadi1@yahoo.fr ; H. Mukalazi: hmukalazi@kyu.ac.ug

ARTICLE IN PRESS

Abstract

Using traditional materials, especially earthen materials and plant waste, is becoming more popular worldwide due to lower construction costs, improved thermal comfort, reduced energy use, and fewer carbon dioxide emissions. In this context, tests have been performed on a stabilized earth bricks (SEBs) made from raw earth bricks combined with *Vicia faba* waste (*Vf*W) and biochar derived from this waste (BVfW), obtained by pyrolysis at 300°C and 500°C, using a factorial design with B*Vf*W contents ranging from 0.5 to 6 wt%. The effects of these compounds on the controlled variables were

ARTICLE IN PRESS

examined using artificial neural network (ANN) techniques and response surface methodology (RSM) to assess the mechanical behavior and thermophysical properties of the bricks within a system that varies the percentage of B*VfW* and pyrolysis temperature. The best conditions were found to be 500°C and 4% B*VfW* content, based on the RSM desirability function and the ANN genetic algorithm. This experimental approach allows for optimizing production conditions by selecting the best parameters to create bricks with balanced strength.

Keywords: Earthen bricks; *Vicia faba*; Mechanical behavior; thermophysical properties; Optimization.

Nomenclature

VfW *Vicia faba* waste
B*VfW* Biochar derived from *Vicia faba* waste
SEBs Stabilized earth bricks
RSM Response Surface Methodology
ANOVA Analysis of Variance
CCD Central Composite Design
DF Desirability function
ANN Artificial Neural Network
MS Mean square
p-value Probability value
F-value Fisher value
SD Standard deviation
MLP Multilayer Perceptron
RMSE Root Mean Square Error
MSE Mean Square Error
R^2 Correlation coefficient
CV Coefficient of variation
AP Adequate precision
3D Three-dimensional

ARTICLE IN PRESS

ARTICLE IN PRESS

2D Two-dimensional
GA genetic algorithm
FS Flexural strength
CS Compressive strength
TC Thermal conductivity
DPW Date palm waste
KNN K-nearest neighbors
CKD Cement kiln dust

1. Introduction

Rising levels of greenhouse gas emissions and air pollution drive climate change, a major global issue that impacts the climate, human health, and the economy. The building sector significantly contributes to CO_2 emissions and consumes a large share of non-renewable energy [1]. Implementing strategies to reduce CO_2 emissions is essential [2]. Energy-saving planning and measures to lower potential emissions must be prioritized to promote a reduction in CO_2 emissions [3]. Reusing materials, minimizing waste, and developing sustainable products are some recent strategies aimed at lowering carbon dioxide emissions and their harmful environmental effects [4–6].In this context, many research studies have been conducted to reduce energy consumption related to air conditioning and heating systems, especially through improving wall thermal insulation and material choice [7,8]. In this context, using raw earth bricks made of bio-based composite materials is a particularly appealing approach. These minimally processed, low-carbon bricks not only decrease building energy requirements but also significantly reduce CO_2 emissions during construction. They are a sustainable option, especially in rural areas, due to their natural ability to regulate indoor temperatures, local availability, and affordability [9,10].

Given the negative environmental effects of cement use, especially regarding CO_2 emissions and energy consumption, clay bricks appear to be a viable and sustainable alternative [11]. They align fully with sustainable building

ARTICLE IN PRESS

principles because they are traditionally made without complex industrial processes. Although there was a decline with the rise of commercial materials, clay, a natural substance mined directly from the earth, has been used for thousands of years in construction and remains popular in poorer countries [12]. The geographical context influences its physical and chemical properties as well as how it is used, with local agricultural resources often affecting the choice of additives. Due to their minimal environmental impact and ability to support more eco-friendly construction, raw earth bricks are increasingly favored in the construction industry, according to numerous studies [13,14]. According to previous research, the mechanical properties of old adobe buildings, such as their compressive and tensile strengths, range from 0.66 to 2.15 MPa and 0.12 to 0.40 MPa, respectively [15]. However, these properties can be improved in adobe stabilized with gypsum, which can achieve a bending strength of over 1.5 MPa and a compressive strength (CS) of 4.72 MPa, as proposed [16]. A study on raw earth bricks reinforced with fibers and chemical stabilizers observed similar patterns [23].

Several recent studies have examined the stabilization of raw earth using natural fibers for building purposes [17–20]. The results confirmed the positive effects of these fibers on the thermomechanical properties of the bricks. Bouhicha et al. [18] observed that if the straw content is ideal, adding straw improves CS while lowering shrinkage and hardening time. Likewise, the researchers found that the straw-reinforced specimen was more ductile than a sample without straw, and they also noted an increase in flexural strength (FS) and shear strength. Furthermore, according to Eslami et al. [21], adobe bricks reinforced with palm fibers perform better mechanically than unreinforced ones, especially in terms of tensile strength and ductility. Interestingly, a fiber percentage of 0.25% yielded the best CS, while tensile strength increased directly with fiber dosage. According to Zak et al. [22], the density of earth bricks mainly determines their CS, while hemp and flax fibers have little effect on strength but significantly alter fracture behavior.

ARTICLE IN PRESS

Conversely, adding gypsum and cement tends to weaken the clay matrix, which greatly reduces CS. Adding fibers to bricks offers an effective way to improve durability and strength. Recent studies have explored various agricultural residues, such as straw, sawdust, and seaweed [23,24], demonstrating that fiber incorporation—ranging from 0.5% to 3%—can enhance flexural and compressive strengths by approximately 30%, often meeting minimum regulatory standards. However, the impact of bio-additives varies; while materials like alfalfa[25] and date palm waste[26] can significantly improve thermal insulation, they may also lead to a reduction in compressive strength if the fiber content exceeds optimal thresholds (typically 0.25% to 2%) [27,28]. Nevertheless, the stabilization of excavated soil with cement and Alfa fibers has shown that achieving high mechanical performance (up to 8.12 MPa) remains possible alongside reduced thermal conductivity [29].

Prioritizing recyclable and environmentally friendly building materials, such as biochar-based insulation and bricks, is essential for a full commitment to sustainable development [30–32]. Biochar, produced by pyrolyzing biomass, is highly useful for building materials and heat generation [33]. Its remarkable qualities—low density, low TC, and high porosity—make it a promising alternative to fossil carbon resources and an effective tool for reducing greenhouse gas emissions [34–37]. As a result, biochar significantly enhances a building's sustainability [38–40]. Recent quantitative assessments demonstrate the magnitude of this impact; for instance, incorporating 30% biochar can sequester approximately 59 kg of CO_2 per tonne of material, effectively achieving a carbon-negative footprint [41]. Furthermore, the global adoption of biochar-based strategies could theoretically mitigate up to 12% of current anthropogenic greenhouse gas emissions [42], highlighting its transformative potential in shifting the construction industry toward a durable carbon sink model [43]. Despite these benefits, this locally available resource remains underutilized in sustainable construction, where it is

ARTICLE IN PRESS

produced from agricultural waste to reinforce raw earth bricks—an achievement the authors claim is a first in the field. Biochar not only increases the value of an organic by-product but also plays a key role in CO_2 sequestration, significantly reducing the carbon footprint of construction materials [44,45]. In the context of earthen construction, such as adobe, the integration of bio-additives is particularly relevant. Unlike conventional fired bricks, adobe bricks are produced without high-temperature firing, resulting in inherently low embodied energy [46]. Enhancing their thermophysical properties through bio-based stabilization—using plant aggregates or biochar—further elevates their status as a high-performance, low-carbon alternative. Recent studies suggest that such reinforcements can improve mechanical resistance and thermal insulation while effectively trapping carbon within the material matrix [47].

To maximize these advantages, new techniques such as artificial neural networks (ANN) and response surface methodology (RSM) have recently been used to optimize the traits of bio-based materials that include biochar. Several studies have demonstrated the effectiveness of digital approaches, such as heuristic frameworks, combined data sets, and K-nearest neighbors (KNN)/ANN metamodels, which have led to the use of RSM and ANN to improve mechanical performance [48,49]. Boumaaza et al. [50] studied the optimization of bio-mortars by replacing part of the cement with biochar produced from pyrolyzing *Washingtonia filifera* waste at different temperatures (300, 400, and 500°C). They examined factors affecting porosity, CS, and TC using RSM. The results show that using 1% biochar pyrolyzed at 500°C results in a TC of 0.52 W/m·K and a CS of 63.81 MPa after 28 days. Based on optimization through RSM and ANN, a ratio of 1% *Washingtonia filifera* waste pyrolyzed at 500°C enhances mechanical performance by 5% in FS, 20% in displacement, and 265% in flexural modulus [51]. Additionally, Nakkeeran et al. [52] utilized ANN and RSM to optimize the properties of Bio-Bricks made from peanut shells and cementitious

ARTICLE IN PRESS

binders. When predicting dry density, CS, and water absorption, the ANN models showed exceptional accuracy (R^2 > 0.99). Using ANN, RSM, and Technique for Order Preference by Similarity to Ideal (TOPSIS) methods, Mebarkia et al. [53] optimized the production of low-temperature clay bricks by adding cement kiln dust (CKD). By testing various proportions of CKD (0–30%) and firing temperatures between 600°C and 900°C, they found optimal conditions—approximately 30% CKD at temperatures ranging from 800°C to 896°C—that improve the thermomechanical properties of the bricks while reducing their environmental impact.

The idea is to conceive an ecological insulation material at very low cost and which can meet the technical requirements in the building sector. Additionally, this study aimed to determine the optimal mixture of these additives to achieve the best performance. To do this, a statistical regression model was created to forecast the mechanical and thermal characteristics of stabilized earth bricks (SEBs) in conjunction with an ANN and RSM. These models take into account the *Vicia faba* waste (*Vf*W) as well as the addition of biochar derived from these waste (B*Vf*W) levels (0.5%, 0.75%, 1%, 2%, 3%, 4%, 5%, and 6%) by weight, pyrolyzed at 300°C and 500°C to the mixture. This research is novel because no previous studies have explored these two methods to predict the mechanical and thermophysical properties of bricks containing biochar. Nevertheless, to the authors' knowledge, no research has been conducted on using *Vf*W and biochar B*Vf*W to produce bricks. Thus, the innovative application of *Vf*W and B*Vf*W biochar makes this study remarkable.

2. Materials and methods

2.1 Materials

The *Vf*, or broad bean, is a legume widely cultivated across Algeria, especially in the Ben Djerrah region, located in the wilaya of Guelma (36°26'04.51"N 7°22'42.05"E). It is an annual plant that grows between 20 and 180 cm tall, with an upright, ribbed stem [54]. Aside from its culinary uses, this plant

ARTICLE IN PRESS

produces a significant amount of agricultural waste, particularly plant fibers from the stems and pods, which can be recycled through a circular economy approach. Bean stalks are transformed using a controlled retting method designed to separate the cellulose fibers. The stems undergo spontaneous bacterial breakdown when kept submerged for around a month at a steady temperature of 30 to 35°C, releasing the fiber bundles from their plant matrix. These fibers provide a renewable and eco-friendly option for the creation of high-performance bio-based materials after being manually removed and dried (**Fig. 1**).

The *Vf*W fibres were pyrolysed to obtain B*Vf*W for use in this research. The pyrolysis technique, which involves heating *Vf* waste in an oxygen-poor atmosphere, is used to produce biochar from these fibers. Through this heat treatment, the biomass is transformed into a stable, carbon-rich material with a highly microporous structure, enabling effective long-term CO_2 sequestration. Following this, they were pyrolyzed for 30 minutes at temperatures of 300°C and 500°C in a sealed oven. The furnace is equipped with a vent system to allow volatile vapors from organic compounds to be released during pyrolysis. Before being used to prepare bio-adobe, the resulting biochar was processed into finer particles using a grinder and cooled in a hermetic container [50]. When used as reinforcement in raw earth bricks, the biochar produced in this manner exhibits interesting physical and chemical properties that enhance its mechanical strength and thermal performance while reducing environmental impact.

Measurements were made in accordance with the NF P 18-560 standard [55] to ascertain the grain-size distribution of the soil. Biochar derived from *Vicia faba* waste (B*Vf*W) has a finer particle distribution than soil, which helps it absorb more into the clay matrix, according to the particle size study (**Fig. 2**). The soil's suitability for earthen construction is confirmed by the fact that the particle-size distribution curve completely fits within the recommended zone given by ASTM D2487 standard [56] for SEBs. A highly compact structure with

ARTICLE IN PRESS

balanced porosity is indicated by the soil's specific gravity of 2520 kg/m³ and apparent density of about 1285 kg/m³. The plasticity of the soil was determined through original laboratory tests following the ASTM D4318 standard [57]. The soil was found to be quite pliable, with a plasticity index of 17% and a liquid limit of 35% according to the Atterberg limits. This classification indicates a clay fraction (particles < 2 µm) of approximately 22%, which plays a fundamental role in the binding behavior and the development of the mechanical strength of the bio-based bricks. During drying and curing, these characteristics maintain shape, compaction, and dimensional stability. At the same time, a finer particle-size distribution is seen in the BC. This implies that adding it to soil mixtures could enhance matrix uniformity and fill up interstitial spaces.

2.2. Bricks manufacturing

Adobe bricks are created by combining clay, water, biochar, and fibers from the *Vicia faba* plant (**Fig. 3**). Brick samples with B*VfW* percentages ranging from 0.5% to 6% were pyrolyzed at 300°C and 500°C with 1% *VfW*. After mixing the dry components for 30 minutes, the mixtures were hydrated until they reached a homogeneous plastic state suitable for optimal compaction. This consistency was carefully controlled to ensure the mixture was moist enough to prevent crumbling while remaining dry enough to avoid sticking to the mold, thus ensuring structural integrity upon demolding. The weight of the bricks is maintained at 850 g, as is that of the fibre (10 g), while the biochar content varies from 0.5% to 6% by weight, or 5 g to 60 g. This biochar is added to the clay to improve the brick's thermomechanical properties. It is produced by pyrolyzing the V_f waste at 300°C and 500°C, turning plant leftovers into a porous carbon material that can permanently trap CO_2.

Water is added to each mixture based on the biochar content, with the water-to-dry-mix ratio ranging from 23.5% (for 0.5% biochar) to 64.7% (for 6% biochar and *Vicia faba* waste). Because biochar is porous and absorbent, it needs more water to create a uniform mixture and facilitate molding, which

ARTICLE IN PRESS

explains the direct relationship between biochar percentage and water amount. While excess water can affect the bricks' cohesiveness and strength, insufficient water can make the mixture less flexible.

To ensure biochar-based bricks maintain good shape, and optimal performance after hardening, water dosage must be adjusted according to the amount of biochar. This precise control allows the full benefits of biochar—especially its mechanical strength, reduced TC, and ability to sequester carbon—to be realized. Bricks made from B*VF*W were produced following the experimental plan (**Table 1**). A total of sixteen distinct brick formulations were prepared and analyzed. These consist of eight different biochar percentages (ranging from 0.5% to 6%) combined with two separate pyrolysis temperatures (300°C and 500°C), as detailed in Table 2. Each combination represents a unique sample set, allowing for a comprehensive evaluation of the interaction between biochar dosage and thermal treatment on the bricks' properties. To ensure experimental consistency, several parameters were kept constant for all formulations: the soil type (Guelma clay), the fiber content (fixed at 1% *VF*W or 10 g), and the total dry weight of each brick (850 g).

2.3. Mechanical and physicothermal properties

Prismatic specimens measuring 40 × 40 × 160 mm^3 were used for bending strength (FS) testing with universal testing equipment Zwick/Roell Z005 at an applied loading rate of 50 N/s in accordance with ASTM C348-14 [58]. The CS experiment was conducted using cubic samples measuring 40 × 40 × 40 [59]. For each combination, a group of three specimens was tested. ASTM C642 [60] was used to measure the accessible porosity to water. From samples submerged in water (M_{water}), saturated with air (M_{air}), and dried in an oven at 90°C (M_{dry}), porosity (P) was calculated using **Equation (1)**:

$$P(\%) = \frac{(M_{air} - M_{dry})}{(M_{air} - M_{water})} \times 100 \quad (1)$$

The European standard ISO 22007-2 [61] describes the slab test process used to assess the TC of bricks. A flatbed thermal conductivity-meter with two

ARTICLE IN PRESS

cooling units at both ends of a heated central element was used to measure a material's TC. Both samples were placed into the spaces within the heating and cooling units to ensure consistent heat transfer. Once the heat transfer stabilized, the coefficient of thermal transfer λ (W/m·K) of each specimen was calculated using **Equation (2)**:

$$\lambda = \frac{Q \times d}{2A(T_1 - T_2)} \quad (2)$$

Q (W) indicates the cooling unit's heating power, d (m) denotes the sample's width, A (m²) represents the thermal transfer region, and T_1 and T_2 (K) are the temperatures of the heating and cooling units, respectively.

The systematic methodology and sequential stages of this research, ranging from material preparation to predictive validation, are outlined in the framework presented in **Fig. 4**.

2.4. *Mathematical Models*

2.4.1. Experiment Design Using Response Surface Methodology (RSM)

RSM is a set of mathematical and statistical methods used to identify relationships between independent parameters and outcomes [62,63]. The central composite design (CCD) was employed to analyze data from bricks reinforced with B*V*W using the Design Expert 13 software. As shown in **Table 1**, The RSM considers two independent factors: B*V*W% (A) and temperature (B). The codes (-1) and (+1) indicate different levels in the experimental design, representing the minimum and maximum values assigned to the center points. Sixteen tests were performed (**Tables 2** and **3**) to establish the process conditions using the RSM/CCD approach. A second-order polynomial equation was used to calculate the compressive stress, flexural stress, and TC based on the independent variables.

$$Y = \beta_0 + \sum_1^k \beta_i X_i + \sum_1^k \beta_{ij} X_i X_j + \sum_1^k \beta_{ii} X_i^2 \quad (3)$$

ARTICLE IN PRESS

In this case, Y represents the experiment's outcome (FS, CS, and TC), X_i and X_j are the independent variables, β_{ij} and β_{ii} denote the interaction effects and quadratic coefficients, respectively, and β_0 and β_i represent the fixed and linear coefficients related to the CCD estimation.

2.4.2. Artificial Neural Network (ANN)

A practical approach for reconstructing the behavior of any nonlinear process is to use ANN modeling [64,65]. The neuronal functions of the human brain are mathematically and numerically mimicked by ANNs [53]. These networks consist of multiple interconnected artificial neurons, each employing a mathematical model to produce a single output based on all its inputs. The neural network that represents the input variables is in the input layer, the hidden layer is in the second layer, and the ANN outputs are in the final layer (output layer), forming a multilayer perceptron (MLP) architecture. The nonlinear variation in transfer (f) is usually associated with the hyperbolic type, as shown in **Equation (4)**:

$$f = \sum_{i=1}^{n} W_i X_i \quad (4)$$

where: W_i represents the adjusting settings, X_i for the neurons' input parameters, and n indicates the number of neurons.

In this study, three MLPs are used independently to predict FS, CS, and TC responses, respectively: 2-5-1, 2-7-1, and 2-8-1. **Fig. 5** shows the structure of the applied MLP. The input layer, the first visible layer, consists of two neurons that process the input data. The second layer, known as the hidden layer, creates a unique model after analyzing the incoming input. It has five, seven, and eight neurons for FS, CS, and TC, respectively. The output layer, which produces the final output, contains a single neuron. The weights and biases of the neurons in the ANN are adjusted during training to minimize the residual error. The Levenberg-Marquardt (LM) algorithm is used in this study to perform this optimization. The ANN outputs a value by applying activation functions to the sum of weighted inputs. The network captures

ARTICLE IN PRESS

nonlinear interactions through the tanh activation functions in the hidden layers.

By calculating the difference between the predicted and observed responses of the network, error ratios evaluate the accuracy of an ANN model. The current ANN model is assessed using the correlation coefficient (R^2). The mean square error (MSE) and root mean square error (RMSE) are two key metrics [66,67]. They are expressed as follows:

$$R^2 = \frac{\sum_1^n((\text{Predictedi-Actual}_i)}{\sum_{i=1}^n((\text{Predictedi-Actual}_i)^2} \quad (5)$$

$$\text{RMSE} = \sum_1^n \sqrt{\frac{(\text{Predictedi-Actual}_i)^2}{n}} \quad (6)$$

$$\text{MSE} = \sum_1^n \frac{(\text{Predictedi-Actual}_i)^2}{n} \quad (7)$$

2.4.3. Applying Genetic Algorithms (GAs) and Artificial Neural Networks (ANN)

Algorithms designed to mimic the evolution of the human genetic system are called genetic algorithm (GA) approaches. To address both linear and nonlinear problems, GA explores all regions and use potential areas by applying mutations, crossovers, and selections to the population members. The GA-ANN model combines two methods: the ANN and the GA.

3. Results and discussions

3.1. Mechanical and thermophysical properties

Fig. 6a illustrates how FS changes with B*VFW* concentration and pyrolysis temperature. The graph shows a non-linear trend: strength steadily increases with biochar content until reaching a maximum at 4%, then declines. The strength rises from 0.52 MPa (0.5%) to 1.33 MPa (4%) at 300°C, then drops to 1.03 MPa (6%). This rise is more prominent at 500°C, reaching 1.47 MPa (4%), before decreasing to 1.13 MPa (6%). This pattern indicates that moderate biochar addition enhances the material's density and internal

ARTICLE IN PRESS

cohesion, likely by strengthening the clay matrix and plugging pores. However, the increase in strength despite rising porosity (**Fig. 6c**) suggests that mechanical performance is not governed by void volume alone, but rather by the quality of the interface between the biochar and the soil matrix.

Temperature plays a decisive role in this mechanism through the chemical and physical transformation of the fibers. At 500°C, the more complete carbonization of the B*VF*W increases the surface roughness and the functional groups of the biochar particles, fostering stronger mechanical interlocking with the clay. Furthermore, at this temperature, the partial thermal activation of clay minerals (dehydroxylation) initiates a pre-sintering process, which compensates for the increased porosity by creating more rigid mineral bridges [68,69]. However, strength decreases more rapidly (≥5%), possibly due to excess carbon particles disrupting the structure and increasing porosity. Temperature also plays an important role: bricks fired at 500°C are stronger than those fired at 300°C at all percentages, implying that higher temperatures promote component reactivity. The FS of the bricks increased from 0.50 MPa for the reference mortar to 0.52 MPa and 0.54 MPa for bricks with B*VF*W pyrolyzed at 300°C and 500°C, respectively, when 0.5% B*VF*W was added. This slight increase suggests that even low levels of biochar can improve load distribution and reduce microcracks, enhancing the matrix.

This finding aligns with research by [70,71], which demonstrated that adding biochar or plant fibers improves mechanical properties up to a certain point, beyond which dispersion becomes uneven and porosity increases. These patterns also match the results of research conducted by Kumar et al. [72], who examined the effect of adding biochar, made up of 90% sawdust and 10% rice husks, to cement paste. Their study shows that FS increases with 3% biochar but decreases at 5% and 10%, indicating an optimal threshold. Conversely, the formulation with 4% B*VF*W and 500°C promotes the recovery of organic waste and reduces environmental impact while maintaining competitive mechanical strength (1.47 MPa).

ARTICLE IN PRESS

Fig. 6b shows how CS of bricks changes with fire temperature and the percentage of B*VF*W. The results indicate that strength gradually increases as biochar content rises to an optimal level of 4%, reaching 4.16 MPa at 300°C and 4.41 MPa at 500°C before decreasing beyond that point. This pattern suggests that biochar helps reinforce the clay matrix, likely due to improved compaction, lower porosity, and positive interactions between carbon particles and mineral binders. It is essential to note that while porosity increases constantly (**Fig. 6c**), CS also increases up to 4%. This decoupling confirms that the "bridging effect" and the internal friction provided by the biochar particles outweigh the negative impact of the voids up to this threshold. The shift from 300°C to 500°C induces a more advanced decomposition of organic volatiles within the fibers, leaving a more stable carbon skeleton that acts as a structural micro-reinforcement.

The effect of temperature is also evident: bricks fired at 500°C have slightly higher strength than those fired at 300°C at each addition rate, indicating better densification and more effective sintering[73,74] . At 500°C, the removal of chemically bound water from the clay matrix improves the chemical affinity between the mineral phase and the biochar surfaces. The best formulations at 4% B*VF*W and 500°C show a 100% increase over the reference brick (2.20 MPa), highlighting the potential of biochar as a mechanical reinforcement. These findings agree with Kumar et al. [72], who observed that adding 3% biochar to cement pastes increased their CS, but it decreased at 5% and 10% due to uneven dispersion and excess porosity. By adding B*VF*W in moderation and controlling pyrolysis temperatures, the bricks' FS and CS can be maximized, while organic waste is recycled in line with sustainable construction principles.

As shown in **Fig. 6c**, the results for porosity as a function of burning temperature and B*VF*W percentage reveal a clear pattern: porosity increases with biochar content, regardless of temperature. The improved formulations reach up to 8.11% at 300°C and 8.24% at 500°C for 6% B*VF*W, while the

ARTICLE IN PRESS

reference brick without biochar has a porosity of 4.96%. The porous nature of biochar itself, which introduces additional voids and changes the material's compactness when incorporated into the matrix, explains this steady increase. The effect is minimal (≈6.4–6.9%) at low levels (0.5–1%), but above 2%, porosity nears 7.5%, indicating matrix saturation and less uniform dispersion. Temperature also influences porosity, though to a lesser extent. For each addition rate, the values at 500°C are slightly higher than those at 300°C. This is attributed to the thermal degradation of residual hemicellulose and cellulose at 500°C, which increases the internal vesicularity of the biochar, and the potential onset of clay dehydroxylation, which generates additional micro-pores. The findings of Kumar et al. [72], which indicate that adding biochar to cementitious materials increases porosity—especially at rates above 5%—are consistent with this trend.

The insulating effect of this material is supported by the TC data, which show a consistent decrease in TC as the biochar percentage increases (**Fig. 6d**). At 300°C and 500°C, the improved formulations reach values as low as 0.36 W/(m·K) from 5% B*VA*W, while the reference brick without biochar has a TC of 0.69 W/(m·K). This reduction is due to biochar's low density and porous structure, which restrict heat transfer through the matrix. TC decreases from 0.69 to 0.36 W/(m·K) between 0 and 6% B*VA*W at 300°C, a drop of over 48%. At 500°C, the decline is similar even though the initial value is slightly higher (0.75 W/(m·K) at 0.5%).

Bricks can be optimized for sustainable and bioclimatic construction by using B*VA*W, which enhances their thermal efficiency and reduces conductivity without significantly compromising their mechanical properties. The B*VA*W-based formulation (4%, 500°C) exhibits a porosity of 7.96%, an FS of 1.47 MPa, a CS of 4.41 MPa, and a TC of 0.39 W/(m·K), all of which align with the latest research findings on biobased bricks. These results support your material's competitiveness for non-load-bearing applications while also reducing carbon emissions and improving thermal insulation.

ARTICLE IN PRESS

The thermal and mechanical properties of the optimized BVFW-based formulation (4%, 500 °C) align with the functional requirements for sustainable and bioclimatic construction. Specifically, the measured compressive strength of 4.41 MPa exceeds the 4.14 MPa (600 psi) threshold established by ASTM C129 [75] for non-load-bearing masonry units. When compared to the reference control specimen (plain soil), which exhibited a compressive strength of 2.20 MPa, a flexural strength of 0.50 MPa, and a thermal conductivity of 0.69 W/(m·K), the optimized brick demonstrates a 100% increase in compression, a 194% gain in flexural strength, and a 48% reduction in thermal conductivity. Combined with a porosity of 7.96% and a low thermal conductivity of 0.39 W/(m·K), these results confirm that BVFW optimization significantly enhances insulation performance while effectively doubling the mechanical resistance required for high-performance non-structural applications.

Fig. 7 shows the fracture surface of stabilized earth bricks containing Vicia faba plant fibres. A ductile failure mode is observed, in which the fibres act as structural bridges across the cracks. Unlike a brittle fracture, which would be clean and smooth, the fibres here ‘stitch’ the earthen matrix together, increasing the material’s ability to absorb energy and resist tensile stress after cracking. The incorporation of biochar complements this structure by densifying the matrix and improving adhesion at the fibre-earth interface. By filling the pores, biochar reduces areas of weakness, allowing for more efficient transmission of stresses to the fibres and thus optimizing the overall mechanical performance of the adobe.

3.2. Response surface methodology (RSM) for flexural strength (FS), compressive strength (CS) and thermal conductivity (TC)

A CCD was performed to assess how process parameters influence the prediction of flexural CS and TC for different brick types. Because of their higher correlation coefficients (R^2), adjusted R^2, and anticipated R^2, the quadratic models meet the previously set selection criteria. The second-

ARTICLE IN PRESS

degree polynomial equations, which predict the responses for FS, CS, and TC based on the CCD experimental design, provide the derived model equations, corresponding to **Equations (8)–(10)**, respectively. These equations effectively explain how the independent parameters relate to the responses, according to the results of the Analysis of Variance (ANOVA).

$$\text{Flexural strength} = 1.3212 + 0.2543\times BVfW + 0.0401\times T + 0.0201\times BVfW\times T - 0.4825\times BVfW^2 + 0.0000\times T^2 \quad (8)$$

$$\text{Compressive strength} = 4.1601 + 0.4013\times BVfW + 0.0556\times T + 0.0294\times BVfW\times T - 1.4103\times BVfW^2 + 0.0000\times T^2 \quad (9)$$

$$\text{Thermal conductivity} = 0.3989 - 0.1428\times BVfW + 0.0197\times T - 0.0244\times BVfW\times T + 0.1199\times BVfW^2 + 0.0000\times T^2 \quad (10)$$

An ANOVA was conducted for each response model to determine the nature and type of relationships among the parameters (**Table 4**). The ANOVA's Fisher values (*F*-values) for the FS, CS, and TC models are 116.11, 188.84, and 75.56, respectively, indicating that these models are highly significant. Additionally, the significance of the model terms is confirmed by the *p*-values, which are less than 0.0001 and well below 0.0500. The qualities of CS, FS, and TC are greatly affected by terms A, B, and A^2 in the current model. For the FS, CS, and TC models in this analysis, the Adequate Precision (AP) values—indicating that the signal-to-noise ratio exceeds four—are 28.6106, 35.9346, and 22.6245, respectively. These values demonstrate that the models are useful in the field of design and suggest an adequate signal.

To assess the relevance and quality of the quadratic models for biochar-based bricks, diagnostic graphs related to test datasets are also essential. The R^2 values for FS, CS, and TC, which are 97.69%, 98.56%, and 96.49%, respectively, show a strong correlation between expected and observed values, demonstrating the models' good fit to different test data. The corresponding adjusted R^2 values are 95.21%, 98.04%, and 96.85%. A reasonable agreement exists for each response when the difference between

ARTICLE IN PRESS

the expected and fitted R^2 values is less than 0.2 [76]. These models can help explore the design space. The standard residual plot suggests a normal distribution of errors, with most values aligned on the right (**Figs. 8a-10a**). As seen in **Figs. 8b–10b**, the correlation between actual and predicted values forms an almost perfect linear line, confirming that these quadratic models are accurate and appropriate for these materials. The experimental results closely match the predictions. As shown in **Figs. 8c-10c**, the linear pattern of residuals indicates a consistent error distribution, suggesting a typical error range with constant variance across responses [77,78]. **Figs. 8d–10d** display the residuals' trend relative to the expected results. The variables FS, CS, and TC can be reliably estimated using the regression equations provided, based on the data above. Therefore, the response models are adequate and suitable for predicting the FS, CS, and TC of bricks.

Fig. 11 shows the response surface and 3D plots of the FS, CS, and TC for the developed model. The properties of the composite bricks are significantly influenced by increasing the biochar content and pyrolysis temperature, as illustrated by the two-dimensional (2D) and 3D curves. The steady rise in FS and CS with biochar content, peaking at around 4%, indicates enhanced internal cohesion and particle adhesion. A high treatment temperature (up to 500°C), which promotes biochar carbonization and improves its compatibility with the clay matrix, supports this trend. Due to its microporous structure, biochar also increases the porosity of the bricks, which is further intensified at higher temperatures and may affect mechanical strength beyond a certain point. The graphs clearly show a decrease in TC with biochar addition, indicating its role as a thermal insulator. The optimal regions where the combined effects of temperature and biochar maximize mechanical performance while minimizing conductivity are highlighted by the 3D response surfaces. These findings align with research [79], which demonstrated that biochar treated between 300°C and 500°C improves the strength, durability, and thermal properties of building materials. Therefore,

ARTICLE IN PRESS

RSM results confirm good agreement between the experimental outcomes and the predictions.

3.3. Artificial neural network (ANN)

In this study, an ANN model was used to calculate the FS, CS, and TC of bricks containing BWW. The input variables for the backpropagation multilayer ANN are temperature (°C) and biochar weight (BWW%), while the recorded FS, CS, and TC values serve as the output layer. During ANN training, feedforward networks with backpropagation—a method that transforms and propagates information from the input layer to the output layer—are commonly employed. The training phase of backpropagation involves multiple steps until the smallest error rate is reached [67,80].

The MATLAB Neural Network Toolbox was used to design the ANN architecture. The input layer of the network has two neurons, while the hidden layers for FS, CS, and TC contain five, seven, and eight neurons, respectively. The final layer, called the exit layer, has a single neuron that produces the output data. Three runs of the dataset were used for testing, validation, and training. The experimental design included sixteen runs: twelve for network training (75%), two for testing (12.5%), and two for validation (12.5%) to evaluate the network's performance. The backpropagation algorithm with a decreasing gradient, a learning rate η = 0.1, and 100 iterations was used for training the neural network. The (TRAINLM) LM algorithms were chosen for their low memory usage and speed. The tangent hyperbolic sigmoid transfer function (TANSIG) was used as the activation function.

Table 5 lists the data sets used for training and testing during model development. The results of analyzing real and projected data are shown in **Fig. 12** and **Table 3** to evaluate the effectiveness of ANN models. It was shown that the expected and actual results align well [81]. For FS, CS, and TC predicted *vs.* actual data, the corresponding R^2 values for the training,

ARTICLE IN PRESS

validation, testing, and overall data sets are 0.9988, 0.9999, 0.9896, and 0.9888; 0.9984, 0.9999, 0.9982, and 0.9986; and 0.9963, 0.9999, 0.9946, and 0.9944. The R^2 for predicted *vs.* actual data on the training, validation, testing, and overall data sets for FS, CS, and TC are 0.9988, 0.9999, 0.9896, and 0.9888; 0.9984, 0.9999, 0.9982, and 0.9986; and 0.9963, 0.9999, 0.9946, and 0.9944. The high R^2 values, all above 0.97, indicate a strong correlation between experimental and expected results.

As a result, the produced ANN models (**Table 6**) could accurately predict reactions because they were based on experimental data. Error rate calculation, which measures the difference between the ANN's predictions and test results, is one of the most important parts of evaluating performance. **Figs. 13a**, **13c**, and **13e** show the zero-error zone, where errors are the lowest. A few errors were intentionally made to demonstrate performance during the ANN network construction phase. At the start of the ANN learning process, the MSE value increased; however, by the end, it decreased. When the best-fit line was aligned with the learning, confirmation, and testing phases, the MSE values for FS, CS, and TC decreased at the 36^{th}, 8^{th}, and 11^{th} epochs, respectively (**Figs. 13b**, **13d**, and **13f**). After that, the ANN training process was completed. This result aligns with previous studies by other researchers, based on earlier published research on the use of ANNs [82–84]. The results show that the models can reliably predict the thermomechanical performance based on selected parameters. This research highlights the effectiveness of using RSM and ANN models to achieve specific performance goals, demonstrating their practical use in brick manufacturing.

3.4. The model's accuracy and usability

The models' validity was further evaluated by comparing the results from RSM and ANN methods. The model generated predictions that closely matched the actual data, as shown by graphs created from all test results. The RSM model's output did not fit the data or match the expected results from the ANN model. Therefore, when extrapolating datasets, the ANN model

ARTICLE IN PRESS

may perform better than the RSM model. The ANN approach allows for accurate prediction and validation of experimental results to assess the thermomechanical properties of bricks. The R^2, MSE, and RMSE metrics were used to assess the suitability of both models. The strong correlation among these metrics indicates that the models are suitable for reproducing real-world outcomes. Generally, a model with an R^2 closer to one is considered more effective at predicting responses [85]. **Table 7** shows the statistical significance and positive results of the ANN and RSM techniques in relation to the observed data. The R^2 values for the ANN model surpass those of the RSM model. Specifically, RSM yields R^2 values of 0.9769, 0.9856, and 0.9649, and MSE values of 0.3032, 0.4653, and 0.4537 for FS, CS, and TC, respectively. Meanwhile, the ANN yields R^2 values of 0.9888, 0.9986, and 0.9944, and MSE values of 0.1043, 0.0213, and 0.1165 for the same parameters. The RMSE errors were also evaluated, showing that the ANN predictions had lower RMSE values compared to the RSM when compared to the actual responses [86].

ARTICLE IN PRESS

3.5. Brick Optimization Using the Response Surface Methodology (RSM)

To determine which of the FS, CS, and TC reactions was most suitable, the RSM approach was used to find optimal values for both parameters (BFW percentage and temperature). The RSM optimization method utilizes the desirability function (DF) of the Design Expert Program. A solution that meets both the lower and upper restrictions is generated through dual-goal optimization [65]. The ideal BFW content and temperature for the FS, CS, and TC results are shown in **Tables 8** and **9** as well as **Fig. 14**. The optimal answers were 1.40 MPa, 4.22 MPa, and 0.38 W/K·m for the FS, CS, and TC values. The results indicated that 4.09% and 500°C were the best values for BFW concentration and temperature, respectively.

3.6. Artificial Neural Network *(ANN) and* genetic algorithm *(GA) technique for variable optimization in clay bricks*

ARTICLE IN PRESS

Genetic mechanisms and biological selection form the basis of GAs. A set of viable starting points (chromosomes) that may be evaluated based on their capacity (fitness) constitutes the first selection point. Three basic techniques used to generate a new set of potential alternatives are selection, crossover, and mutation [87]. To improve tensile characteristics and identify the optimal temperature and B*VF*W percentage, this study employs a GA technique. Compared to mathematical models developed with ANNs, this approach's remarkable predictability led to its selection. The mutation, crossover, and overall population adjustment rates for the GA were 0.01, 100, and 0.70, respectively. The crossover, selection, and mutation methods were chosen using heuristic, roulette, and uniform approaches. ANN was used as a fitness indicator to determine the best options after analyzing the methods for FS, CS, and TC over 100 iterations. **Table 9** displays the optimal variable values (B*VF*W content = 4% and temperature = 500°C) and the ideal responses of TC, FS, and CS, which are 0.37 W/K·m, 1.44 MPa, and 4.36 MPa, respectively. The results showed that the ANN/GA method produced the highest CS (4.36 MPa) and FS (1.44 MPa) compared to CS (4.22 MPa) and FS (1.40 MPa) obtained with RSM/DF. For both methods, the optimal B*VF*W content and temperature levels were similar. The slightly better performance of ANN/GA is due to its ability to capture nonlinear and complex relationships between outcomes and input parameters. RSM/DF is recommended for faster and simpler optimization due to its basic polynomial modeling approach. Conversely, ANN/GA is better suited for complex systems requiring higher precision, as it can model nonlinear data patterns [88].

3. Conclusion

This research emphasizes the potential of bio-sourced materials as a durable building option, particularly raw earth bricks reinforced with *Vicia faba* waste and biochar made from this waste (B*VF*W). It was possible to assess the effects of biochar percentage (0.5–6%) and pyrolysis temperature (300–500°C) on the thermophysical and mechanical properties of bricks using an

ARTICLE IN PRESS

experimental approach with a factorial design combined with Response Surface Methodology (RSM) and Artificial Neural Network (ANN) optimization techniques. The results lead to the following conclusions:

- The proportion of biochar significantly influenced mechanical strength. It peaked at 4% and then decreased at higher percentages due to increased porosity.
- The biochar component greatly enhanced flexural strength, reaching 1.47 MPa at 4% BVAW and 500°C, compared to 0.5 MPa for the control bricks. Similarly, under optimal conditions, compressive strength increased from 2.20 MPa (without biochar) to 4.41 MPa, showing a notable improvement in the material's internal cohesion.
- As biochar content increased, thermal conductivity (TC) decreased from 0.69 W/m·K to 0.36 W/m·K, indicating that its microporous structure acts as an insulating agent.
- Using the full factorial approach, new quadratic models for mechanical strength and TC were successfully developed, with correlation coefficients (R^2) as high as 96.5%.
- The ideal manufacturing conditions were found at 500°C and 4% BVAW using multi-criteria optimization, ensuring the best balance between heat and mechanical performance.
- ANN proved more reliable for predicting brick properties than RSM, with models showing lower prediction errors (both Root Mean Square Error and Mean Squared Error) and higher R^2 (> 0.98).

The hybrid VAW/BVAW coupling increases the energy efficiency and environmental sustainability of SEBs while recycling local plant waste and helping to reduce carbon footprints, improve thermal comfort, and utilize agricultural waste in line with the circular economy concept. To verify their practical application, long-term research, life cycle analysis, full-scale validation in a Mediterranean climate, and durability testing during repeated wetting-drying cycles are required. Additionally, while the current

ARTICLE IN PRESS

formulation is optimized for non-load-bearing partitions, further research focusing on the optimization of the binder matrix or compaction pressure could extend the applicability of these bricks to load-bearing masonry systems, thereby broadening their structural impact in sustainable construction.

Declarations

Ethics approval and consent to participate: Not applicable

Consent for publication: Not applicable

Data Availability Statement:

The datasets generated and/or analysed during the current study are available from the corresponding author on reasonable request.

Competing interests:

The authors declare that they have no financial interests. All authors certify that they have no other affiliations with or non-financial interest in the subject matter or materials discussed in this manuscript that could be perceived as influencing the submitted work.

Funding: No funding was received for conducting this study.

Acknowledgements: The authors acknowledge the financial support through Ongoing Research Funding program (ORF-2026-688), King Saud University, Riyadh, Saudi Arabia.

Clinical trial number: Not applicable.

Author Contribution

Nadia Frioui: Investigation, Methodology, Conceptualization, Formal analysis, Writing – review & editing

Messaouda Boumaaza: Investigation, Methodology, Conceptualization, Formal analysis, Writing – review & editing

Ahmed Belaadi: Investigation, Methodology, Conceptualization, Formal analysis, Writing – review & editing

Mahmood M. S. Abdullah: Investigation, Writing - review & editing.

Djamel Ghernaout: Investigation, Writing - review & editing.

Amar Al-Khawlani: Investigation, Writing - review & editing.

Herbert Mukalazi: Investigation, Writing - review & editing.

References

[1] L. Huang, G. Krigsvoll, F. Johansen, Y. Liu, X. Zhang, Carbon emission of global construction sector, Renewable and Sustainable Energy Reviews 81 (2018) 1906–1916. https://doi.org/https://doi.org/10.1016/j.rser.2017.06.001.

ARTICLE IN PRESS

[2] L.J.R. Nunes, The Rising Threat of Atmospheric CO2: A Review on the Causes, Impacts, and Mitigation Strategies, Environments - MDPI 10 (2023). https://doi.org/10.3390/environments10040066.

[3] M. Ma, X. Ma, W. Cai, W. Cai, Carbon-dioxide mitigation in the residential building sector: A household scale-based assessment, Energy Convers. Manag. 198 (2019) 111915. https://doi.org/https://doi.org/10.1016/j.enconman.2019.111915.

[4] M. Yang, L. Chen, J. Wang, G. Msigwa, A.I. Osman, S. Fawzy, D.W. Rooney, P.-S. Yap, Circular economy strategies for combating climate change and other environmental issues, Environ. Chem. Lett. 21 (2023) 55–80. https://doi.org/10.1007/s10311-022-01499-6.

[5] A. Almusaed, I. Yitmen, J.A. Myhren, A. Almssad, Assessing the Impact of Recycled Building Materials on Environmental Sustainability and Energy Efficiency: A Comprehensive Framework for Reducing Greenhouse Gas Emissions, Buildings 14 (2024). https://doi.org/10.3390/buildings14061566.

[6] O. Onuaguluchi, N. Banthia, Scrap tire steel fiber as a substitute for commercial steel fiber in cement mortar: Engineering properties and cost-benefit analyses, Resour. Conserv. Recycl. 134 (2018) 248–256. https://doi.org/https://doi.org/10.1016/j.resconrec.2018.03.014.

[7] G.A. Abanto, M. Karkri, G. Lefebvre, M. Horn, J.L. Solis, M.M. Gómez, Thermal properties of adobe employed in Peruvian rural areas: Experimental results and numerical simulation of a traditional bio-composite material, Case Studies in Construction Materials 6 (2017) 177–191. https://doi.org/https://doi.org/10.1016/j.cscm.2017.02.001.

[8] K.S.D. Chandhran, S. Elavenil, A comprehensive state-of-the-art review of sustainable thermal insulation system used in external walls for reduction in energy consumption in buildings, Int. J. Green Energy 20 (2023) 895–913. https://doi.org/10.1080/15435075.2022.2120769.

[9] M. Costi de Castrillo, M. Philokyprou, I. Ioannou, Comparison of adobes from pre-history to-date, J. Archaeol. Sci. Rep. 12 (2017) 437–448. https://doi.org/https://doi.org/10.1016/j.jasrep.2017.02.009.

[10] Y. Kulshreshtha, Nelson.J.A. Mota, K.S. Jagadish, J. Bredenoord, P.J. Vardon, M.C.M. van Loosdrecht, H.M. Jonkers, The potential and current status of earthen material for low-cost housing in rural India, Constr.

ARTICLE IN PRESS

Build. Mater. 247 (2020) 118615. https://doi.org/https://doi.org/10.1016/j.conbuildmat.2020.118615.

[11] Z. He, A. Shen, H. Wu, W. Wang, L. Wang, C. Yao, J. Wu, Research progress on recycled clay brick waste as an alternative to cement for sustainable construction materials, Constr. Build. Mater. 274 (2021) 122113. https://doi.org/https://doi.org/10.1016/j.conbuildmat.2020.122113.

[12] G. Ascensão, J. Pereira, J. Fonseca, A. Costa, V.M. Ferreira, H. Paiva, Reviving heritage with contemporary solutions for adobe wall rehabilitation, Constr. Build. Mater. 458 (2025) 139557. https://doi.org/https://doi.org/10.1016/j.conbuildmat.2024.139557.

[13] M.R. Maaze, S. Shrivastava, Selection of eco-friendly alternative brick for sustainable development; A study on Technical, Economic, Environmental and Social feasibility, Constr. Build. Mater. 408 (2023) 133808. https://doi.org/https://doi.org/10.1016/j.conbuildmat.2023.133808.

[14] I.I. Obianyo, A.A. Mahamat, T.T. Stanislas, G.O. Ihekweme, S.E. Kelechi, K.C. Onyelowe, A.P. Onwualu, A.B.O. Soboyejo, Production and utilization of earth-based bricks for sustainable building applications in Nigeria: status, benefits, challenges and way forward, Journal of Building Pathology and Rehabilitation 6 (2021) 37. https://doi.org/10.1007/s41024-021-00131-4.

[15] D. Silveira, H. Varum, A. Costa, T. Martins, H. Pereira, J. Almeida, Mechanical properties of adobe bricks in ancient constructions, Constr. Build. Mater. 28 (2012) 36–44. https://doi.org/https://doi.org/10.1016/j.conbuildmat.2011.08.046.

[16] N. Degirmenci, The using of waste phosphogypsum and natural gypsum in adobe stabilization, Constr. Build. Mater. 22 (2008) 1220–1224. https://doi.org/https://doi.org/10.1016/j.conbuildmat.2007.01.027.

[17] G. Calatan, A. Hegyi, C. Dico, C. Mircea, Determining the Optimum Addition of Vegetable Materials in Adobe Bricks, Procedia Technology 22 (2016) 259–265. https://doi.org/https://doi.org/10.1016/j.protcy.2016.01.077.

[18] A.C. Abdullah, C.C. Lee, Effect of Treatments on Properties of Cement-fiber Bricks Utilizing Rice Husk, Corncob and Coconut Coir, Procedia

ARTICLE IN PRESS

Eng. 180 (2017) 1266–1273. https://doi.org/https://doi.org/10.1016/j.proeng.2017.04.288.

[19] A. Vatani Oskouei, M. Afzali, M. Madadipour, Experimental investigation on mud bricks reinforced with natural additives under compressive and tensile tests, Constr. Build. Mater. 142 (2017) 137–147. https://doi.org/https://doi.org/10.1016/j.conbuildmat.2017.03.065.

[20] Y. Li, K. Wen, L. Li, W. Huang, C. Bu, F. Amini, Experimental investigation on compression resistance of bio-bricks, Constr. Build. Mater. 265 (2020) 120751. https://doi.org/https://doi.org/10.1016/j.conbuildmat.2020.120751.

[21] A. Eslami, H. Mohammadi, H. Mirabi Banadaki, Palm fiber as a natural reinforcement for improving the properties of traditional adobe bricks, Constr. Build. Mater. 325 (2022) 126808. https://doi.org/https://doi.org/10.1016/j.conbuildmat.2022.126808.

[22] P. Zak, T. Ashour, A. Korjenic, S. Korjenic, W. Wu, The influence of natural reinforcement fibers, gypsum and cement on compressive strength of earth bricks materials, Constr. Build. Mater. 106 (2016) 179–188. https://doi.org/https://doi.org/10.1016/j.conbuildmat.2015.12.031.

[23] E. Olacia, A.L. Pisello, V. Chiodo, S. Maisano, A. Frazzica, L.F. Cabeza, Sustainable adobe bricks with seagrass fibres. Mechanical and thermal properties characterization, Constr. Build. Mater. 239 (2020) 117669. https://doi.org/https://doi.org/10.1016/j.conbuildmat.2019.117669.

[24] M. Costi de Castrillo, M. Philokyprou, I. Ioannou, Comparison of adobes from pre-history to-date, J. Archaeol. Sci. Rep. 12 (2017) 437–448. https://doi.org/https://doi.org/10.1016/j.jasrep.2017.02.009.

[25] Y. Azalam, A. Alioui, N. Al armouzi, M. Benfars, M. Mabrouki, E.M. Bendada, Physical and mechanical properties of adobe bricks reinforced by natural additives, a case study of alfalfa fibers, EUREKA: Physics and Engineering (2024) 144–159. https://doi.org/10.21303/2461-4262.2024.003426.

[26] D. Khoudja, B. Taallah, O. Izemmouren, S. Aggoun, O. Herihiri, A. Guettala, Mechanical and thermophysical properties of raw earth bricks incorporating date palm waste, Constr. Build. Mater. 270 (2021) 121824. https://doi.org/https://doi.org/10.1016/j.conbuildmat.2020.121824.

ARTICLE IN PRESS

[27] O. Ige, H. Danso, Physico-mechanical and thermal gravimetric analysis of adobe masonry units reinforced with plantain pseudo-stem fibres for sustainable construction, Constr. Build. Mater. 273 (2021) 121686. https://doi.org/https://doi.org/10.1016/j.conbuildmat.2020.121686.

[28] C. Babé, D.K. Kidmo, A. Tom, R.R.N. Mvondo, B. Kola, N. Djongyang, Effect of neem (Azadirachta Indica) fibers on mechanical, thermal and durability properties of adobe bricks, Energy Reports 7 (2021) 686–698. https://doi.org/https://doi.org/10.1016/j.egyr.2021.07.085.

[29] N. Gueffaf, B. Rabehi, M. Boumaaza, K. Boumchedda, A. Belaadi, M. M. S. Abdullah, I. Klimkina, H. A. al-Lohedan, A. Al-Khawlani, Y. Chetbani, Performance of Earth Blocks Based on Recycled Dam Sediment and Reinforced with Alfa Fibers : Experimental Study, Journal of Natural Fibers 22 (2025) 2512002. https://doi.org/10.1080/15440478.2025.2512002.

[30] A.I. Osman, M. Farghali, Y. Dong, J. Kong, M. Yousry, A.K. Rashwan, Z. Chen, A. Al-Fatesh, D.W. Rooney, P.-S. Yap, Reducing the carbon footprint of buildings using biochar-based bricks and insulating materials: a review, Environ. Chem. Lett. 22 (2024) 71–104. https://doi.org/10.1007/s10311-023-01662-7.

[31] M. Deshmukh, M. Yadav, Optimizing Thermal Efficiency of Building Envelopes with Sustainable Composite Materials, Buildings 15 (2025). https://doi.org/10.3390/buildings15020230.

[32] Y. Zhang, M. He, L. Wang, J. Yan, B. Ma, X. Zhu, Y.S. Ok, V. Mechtcherine, D.C.W. Tsang, Biochar as construction materials for achieving carbon neutrality, Biochar 4 (2022) 59. https://doi.org/10.1007/s42773-022-00182-x.

[33] A.I. Osman, S. Fawzy, M. Farghali, M. El-Azazy, A.M. Elgarahy, R.A. Fahim, M.I.A.A. Maksoud, A.A. Ajlan, M. Yousry, Y. Saleem, D.W. Rooney, Biochar for agronomy, animal farming, anaerobic digestion, composting, water treatment, soil remediation, construction, energy storage, and carbon sequestration: a review, Environ. Chem. Lett. 20 (2022) 2385–2485. https://doi.org/10.1007/s10311-022-01424-x.

[34] A. Chen, F. Chen, C. Ding, X. Shi, Effect of biochar and sisal fiber on compressive strength of expansive soil, Case Studies in Construction Materials 23 (2025) e05071. https://doi.org/https://doi.org/10.1016/j.cscm.2025.e05071.

ARTICLE IN PRESS

[35] A.I. Osman, M. Farghali, I. Ihara, A.M. Elgarahy, A. Ayyad, N. Mehta, K.H. Ng, E.M. Abd El-Monaem, A.S. Eltaweil, M. Hosny, S.M. Hamed, S. Fawzy, P.-S. Yap, D.W. Rooney, Materials, fuels, upgrading, economy, and life cycle assessment of the pyrolysis of algal and lignocellulosic biomass: a review, Environ. Chem. Lett. 21 (2023) 1419–1476. https://doi.org/10.1007/s10311-023-01573-7.

[36] K. Weber, P. Quicker, Properties of biochar, Fuel 217 (2018) 240–261. https://doi.org/https://doi.org/10.1016/j.fuel.2017.12.054.

[37] S. Gupta, A. Kashani, A.H. Mahmood, T. Han, Carbon sequestration in cementitious composites using biochar and fly ash – Effect on mechanical and durability properties, Constr. Build. Mater. 291 (2021) 123363. https://doi.org/https://doi.org/10.1016/j.conbuildmat.2021.123363.

[38] A. Kumar, T. Bhattacharya, Biochar: a sustainable solution, Environ. Dev. Sustain. 23 (2021) 6642–6680. https://doi.org/10.1007/s10668-020-00970-0.

[39] S. Gupta, H.W. Kua, S.D. Pang, Effect of biochar on mechanical and permeability properties of concrete exposed to elevated temperature, Constr. Build. Mater. 234 (2020) 117338. https://doi.org/https://doi.org/10.1016/j.conbuildmat.2019.117338.

[40] D. Cuthbertson, U. Berardi, C. Briens, F. Berruti, Biochar from residual biomass as a concrete filler for improved thermal and acoustic properties, Biomass Bioenergy 120 (2019) 77–83. https://doi.org/https://doi.org/10.1016/j.biombioe.2018.11.007.

[41] L. Chen, Y. Zhang, L. Wang, S. Ruan, J. Chen, H. Li, J. Yang, V. Mechtcherine, D.C.W. Tsang, Biochar-augmented carbon-negative concrete, Chemical Engineering Journal 431 (2022) 133946. https://doi.org/https://doi.org/10.1016/j.cej.2021.133946.

[42] D. Woolf, J.E. Amonette, F.A. Street-Perrott, J. Lehmann, S. Joseph, Sustainable biochar to mitigate global climate change, Nat. Commun. 1 (2010) 56. https://doi.org/10.1038/ncomms1053.

[43] J. Lehmann, A. Cowie, C.A. Masiello, C. Kammann, D. Woolf, J.E. Amonette, M.L. Cayuela, M. Camps-Arbestain, T. Whitman, Biochar in climate change mitigation, Nat. Geosci. 14 (2021) 883–892. https://doi.org/10.1038/s41561-021-00852-8.

ARTICLE IN PRESS

[44] S. Gupta, H.W. Kua, Biochar as a carbon sequestering construction material in cementitious mortar, Academic Journal of Civil Engineering 35 (2017). https://doi.org/10.26168/icbbm2017.85.

[45] A.I. Osman, M. Farghali, Y. Dong, J. Kong, M. Yousry, A.K. Rashwan, Z. Chen, A. Al-Fatesh, D.W. Rooney, P.-S. Yap, Reducing the carbon footprint of buildings using biochar-based bricks and insulating materials: a review, Environ. Chem. Lett. 22 (2024) 71–104. https://doi.org/10.1007/s10311-023-01662-7.

[46] A. Alioui, S. Idrissi Kaitouni, Y. Azalam, N. Al armouzi, E.M. Bendada, M. Mabrouki, Effect of straw fibers addition on hygrothermal and mechanical properties of carbon-free adobe bricks: From material to building scale in a semi-arid climate, Build. Environ. 255 (2024) 111380. https://doi.org/https://doi.org/10.1016/j.buildenv.2024.111380.

[47] Y. Azalam, A. Alioui, N. Al Armouzi, M. Benfars, M. Mabrouki, E.M. Bendada, Physical and mechanical properties of adobe bricks reinforced by natural additives, a case study of alfalfa fibers, EUREKA, Physics and Engineering 2024-July (2024) 144–159. https://doi.org/10.21303/2461-4262.2024.003426.

[48] B.X. Chai, B. Eisenbart, M. Nikzad, B. Fox, A. Blythe, K.H. Bwar, J. Wang, Y. Du, S. Shevtsov, Application of KNN and ANN Metamodeling for RTM Filling Process Prediction, Materials 16 (2023). https://doi.org/10.3390/ma16186115.

[49] B.X. Chai, J. Wang, T.K.M. Dang, M. Nikzad, B. Eisenbart, B. Fox, Comprehensive Composite Mould Filling Pattern Dataset for Process Modelling and Prediction, Journal of Composites Science 8 (2024). https://doi.org/10.3390/jcs8040153.

[50] M. Boumaaza, A. Belaadi, H. Alshahrani, M. Bourchak, M. Jawaid, Response Surface Methodology Optimization of Palm Rachis Biochar Content and Temperature Effects on Predicting Bio-Mortar Compressive Strength, Porosity and Thermal Conductivity, Journal of Natural Fibers 20 (2023) 2162184. https://doi.org/10.1080/15440478.2022.2162184.

[51] M. Boumaaza, A. Belaadi, M. Bourchak, M. Jawaid, S. Hamid, Comparative study of flexural properties prediction of Washingtonia filifera rachis biochar bio-mortar by ANN and RSM models, Constr. Build. Mater. 318 (2022) 125985. https://doi.org/10.1016/J.CONBUILDMAT.2021.125985.

ARTICLE IN PRESS

[52] G. Nakkeeran, L. Krishnaraj, P. Shakor, G.U. Alaneme, O.N. Otu, Mechanical properties optimization and cost analysis of agricultural waste as an alternative in brick production, Sci. Rep. 14 (2024) 24075. https://doi.org/10.1038/s41598-024-74970-9.

[53] R. Mebarkia, M. Bouzeroura, M. Boumaaza, N. Chelouah, A. Belaadi, I.M.H. Alshaikh, Y. Chetbani, D. Ghernaout, Upcycling cement kiln dust for manufacturing clay bricks fired at different temperatures: RSM and ANN-GA hybrid-optimization, Results in Engineering 27 (2025) 105683. https://doi.org/https://doi.org/10.1016/j.rineng.2025.105683.

[54] M. Benarab, A. Belaadi, A. Bedjaoui, M. Boumaaza, D. Ghernaout, Characterizing novel cellulosic fibers extracted from Vicia faba plant waste stems as a promising reinforcement for applications in sustainable textile and lightweight biocomposites, Int. J. Biol. Macromol. 307 (2025) 141940. https://doi.org/https://doi.org/10.1016/j.ijbiomac.2025.141940.

[55] P. NF, P 18-560: Granulats-Analyse granulométrique par tamisage, AFNOR, Paris (1990).

[56] ASTM D2487, Standard practice for classification of soils for engineering purposes (unified soil classification system) 1, ASTM international, 2017.

[57] D. 4318 ASTM, Standard test methods for liquid limit, plastic limit, and plasticity index of soils, D4318-10 (2010) 0.

[58] ASTM, C348-14 Standard Test Method for Flexural Strength of Hydraulic-Cement Mortars, ASTM International (2008).

[59] ASTM, C109, Standard test method for compressive strength of hydraulic cement mortars, ASTM International, (2008).

[60] C. Astm, Standard test method for density, absorption, and voids in hardened concrete, C642-13 (2013).

[61] ISO 22007-2., Plastics: determination of thermal conductivity and thermal diffusivity: transient plane heat method, International Organization for Standardization, 2008.

[62] D. Sinkhonde, R.O. Onchiri, W.O. Oyawa, J.N. Mwero, Response surface methodology-based optimisation of cost and compressive strength of rubberised concrete incorporating burnt clay brick powder, Heliyon 7 (2021). https://doi.org/10.1016/j.heliyon.2021.e08565.

ARTICLE IN PRESS

[63] L. Li, Y. Wan, S. Chen, W. Tian, W. Long, J. Song, Prediction of optimal ranges of mix ratio of self-compacting mortars (SCMs) based on response surface method (RSM), Constr. Build. Mater. 319 (2022) 126043. https://doi.org/https://doi.org/10.1016/j.conbuildmat.2021.126043.

[64] O.M. Ofuyatan, O.B. Agbawhe, D.O. Omole, C.A. Igwegbe, J.O. Ighalo, RSM and ANN modelling of the mechanical properties of self-compacting concrete with silica fume and plastic waste as partial constituent replacement, Cleaner Materials 4 (2022) 100065. https://doi.org/https://doi.org/10.1016/j.clema.2022.100065.

[65] B.X. Chai, B. Eisenbart, M. Nikzad, B. Fox, A. Blythe, P. Blanchard, J. Dahl, A novel heuristic optimisation framework for radial injection configuration for the resin transfer moulding process, Compos. Part A Appl. Sci. Manuf. 165 (2023) 107352. https://doi.org/10.1016/J.COMPOSITESA.2022.107352.

[66] A. Khelifi, M. Boumaaza, A. Belaadi, D. Tarek, A.R.G. de Azevedo, M. Bourchak, M. Jawaid, Effects of alkaline treatment of Washingtonia mesh waste on the mechanical and physical properties of bio-mortar: experimental and prediction models, Biomass Convers. Biorefin. 14 (2024) 10621–10650. https://doi.org/10.1007/s13399-023-04221-w.

[67] A. Belaadi, M. Boumaaza, H. Alshahrani, M. Bourchak, Optimization of Palm Rachis Biochar Waste Content and Temperature Effects on Predicting Bio-Mortar : ANN and RSM Modelling, Journal of Natural Fibers 20 (2023) 2151547. https://doi.org/10.1080/15440478.2022.2151547.

[68] G. Cultrone, E. Sebastián, K. Elert, M.J. de la Torre, O. Cazalla, C. Rodriguez–Navarro, Influence of mineralogy and firing temperature on the porosity of bricks, J. Eur. Ceram. Soc. 24 (2004) 547–564. https://doi.org/https://doi.org/10.1016/S0955-2219(03)00249-8.

[69] G. Paul, S. Kuppusamy, A.L. Pauline, K. Sellappa, Sustainable biochar-based bricks: evaluating the mechanical, thermal and durability properties of paddy stubble biochar for structural applications, Innovative Infrastructure Solutions 11 (2026) 153. https://doi.org/10.1007/s41062-026-02569-2.

[70] M. Abdulkareem, F. Ayeronfe, T.M. Jassam, A.H. AlAteah, K.A.A. Al-Sodani, M.M.H. Al-Tholaia, H. Yam, A. Ganiyu, S.C. Alih, Compressive

ARTICLE IN PRESS

and Flexural Strengths of Bio-Recycled Concrete Incorporated with Kenaf Fibre, Journal of Natural Fibers 21 (2024) 2296913. https://doi.org/10.1080/15440478.2023.2296913.

[71] Y.M. Tiwari, S.K. Sarangi, A.K. Singh, P. Senthamaraikannan, I. Suyambulingam, R. Kumar, Mechanical, Morphological and Hygroscopic Characterization of Bio-Composites Reinforced with Untreated and Alkali-Treated Grewia flavescens Fibers, Journal of Natural Fibers 22 (2025) 2502649. https://doi.org/10.1080/15440478.2025.2502649.

[72] A. Kumar, A. Pippal, R. Agarwal, R. Kumar, S.N. Bhanavath, H. Athar, S. Kushwah, Thermo-physical study of biochar mixture into the cement based material for thermal comfort, Journal of Building Design and Environment (2023). https://doi.org/10.37155/2811-0730-0201-13.

[73] M. Boumaaza, A. Belaadi, M. Bourchak, K.A. Juhany, M. Jawaid, M.T. Marvila, A.R.G. de Azevedo, Optimization of flexural properties and thermal conductivity of Washingtonia plant biomass waste biochar reinforced bio-mortar, Journal of Materials Research and Technology 23 (2023) 3515–3536. https://doi.org/https://doi.org/10.1016/j.jmrt.2023.02.009.

[74] Y. Zhang, M. He, L. Wang, J. Yan, B. Ma, X. Zhu, Y.S. Ok, V. Mechtcherine, D.C.W. Tsang, Biochar as construction materials for achieving carbon neutrality, Biochar 4 (2022) 59. https://doi.org/10.1007/s42773-022-00182-x.

[75] ASTM C129, Standard Specification for Nonloadbearing Concrete Masonry Units 1, Changes 4 (2003) 1–3.

[76] M. Boumaaza, A. Belaadi, H. Alshahrani, M.K.A. Khan, M. Jawaid, Environmentally mortar development using Washingtonia/biochar waste hybrid: mechanical and thermal properties, Biomass Convers. Biorefin. (2023). https://doi.org/10.1007/s13399-023-04743-3.

[77] L. Li, Y. Wan, S. Chen, W. Tian, W. Long, J. Song, Prediction of optimal ranges of mix ratio of self-compacting mortars (SCMs) based on response surface method (RSM), Constr. Build. Mater. 319 (2022) 126043. https://doi.org/https://doi.org/10.1016/j.conbuildmat.2021.126043.

[78] S. Rocha, G. Ascensão, L. Maia, Exploring Design Optimization of Self-Compacting Mortars with Response Surface Methodology, Applied Sciences 13 (2023). https://doi.org/10.3390/app131810428.

ARTICLE IN PRESS

[79] H. Xie, X. Zhou, Y. Zhang, W. Yan, Prediction of biochar characteristics and optimization of pyrolysis process by response surface methodology combined with artificial neural network, Biomass Convers. Biorefin. 15 (2025) 4745–4757. https://doi.org/10.1007/s13399-023-05194-6.

[80] A.B. Çolak, K. Akçaözoğlu, S. Akçaözoğlu, G. Beller, Artificial Intelligence Approach in Predicting the Effect of Elevated Temperature on the Mechanical Properties of PET Aggregate Mortars: An Experimental Study, Arab. J. Sci. Eng. 46 (2021) 4867–4881. https://doi.org/10.1007/s13369-020-05280-1.

[81] M. Sarıdemir, Predicting the compressive strength of mortars containing metakaolin by artificial neural networks and fuzzy logic, Advances in Engineering Software 40 (2009) 920–927. https://doi.org/https://doi.org/10.1016/j.advengsoft.2008.12.008.

[82] D.J. Armaghani, P.G. Asteris, A comparative study of ANN and ANFIS models for the prediction of cement-based mortar materials compressive strength, Neural Comput. Appl. 33 (2021) 4501–4532. https://doi.org/10.1007/s00521-020-05244-4.

[83] A. Kooshkaki, H. Eskandari-Naddaf, Effect of porosity on predicting compressive and flexural strength of cement mortar containing micro and nano-silica by multi-objective ANN modeling, Constr. Build. Mater. 212 (2019) 176–191. https://doi.org/https://doi.org/10.1016/j.conbuildmat.2019.03.243.

[84] H. Eskandari-Naddaf, R. Kazemi, ANN prediction of cement mortar compressive strength, influence of cement strength class, Constr. Build. Mater. 138 (2017) 1–11. https://doi.org/https://doi.org/10.1016/j.conbuildmat.2017.01.132.

[85] X. Li, C.M. Ho, S.I. Doh, M.I. Al Biajawi, Q. Ma, D. Zhao, R. Liu, Strength Characteristics and Prediction of Ternary Blended Cement Building Material Using RSM and ANN, Buildings 15 (2025). https://doi.org/10.3390/buildings15050733.

[86] E. Aydoğmuş, H. Arslanoğlu, M. Dağ, Production of waste polyethylene terephthalate reinforced biocomposite with RSM design and evaluation of thermophysical properties by ANN, Journal of Building Engineering 44 (2021) 103337. https://doi.org/https://doi.org/10.1016/j.jobe.2021.103337.

ARTICLE IN PRESS

[87] Z. Wang, A. Sobey, A comparative review between Genetic Algorithm use in composite optimisation and the state-of-the-art in evolutionary computation, Compos. Struct. 233 (2020) 111739. https://doi.org/https://doi.org/10.1016/j.compstruct.2019.111739.

[88] Y. Wang, A.A. AL-Huqail, S. Salimimoghadam, K. Jasim Mohammed, A. Jan, H.E. Ali, M. Amine Khadimallah, H. Assilzadeh, The metaheuristic optimization of the mechanical properties of sustainable energies using artificial neural networks and genetic algorithm: A case study by eggshell fine waste, Int. J. Energy Res. 46 (2022) 21338–21352. https://doi.org/https://doi.org/10.1002/er.8255.

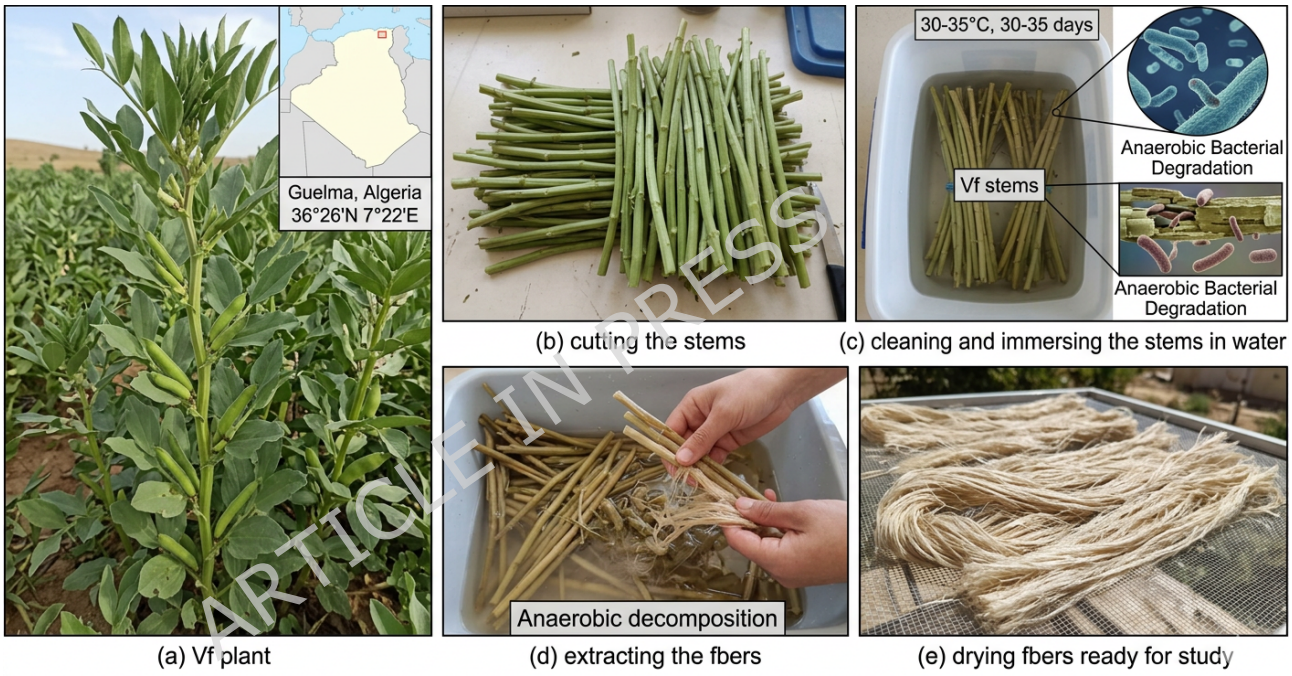

Fig. 1. Processes involved in obtaining *Vicia faba* fibers : (a) *Vf* plant; (b) cutting the stems; (c) cleaning and submerging the stems in water; (d) extracting the fibers; and (e) drying the fibers before they may be studied.

ARTICLE IN PRESS

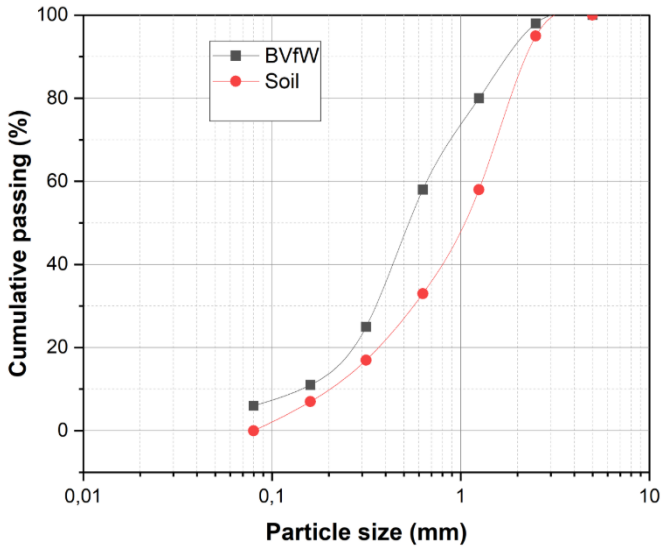

Fig. 2. Soil and biochar particle size analysis used in brick construction.

Fig. 3. (a) Raw *clay* , (b) *Vicia faba* waste (B*Vf*W), (c) biochar made from *Vicia faba* waste (B*Vf*W), (d) weighing of clay, biochar, and water components, (e) samples for flexural test and (f) samples for compression test.

ARTICLE IN PRESS

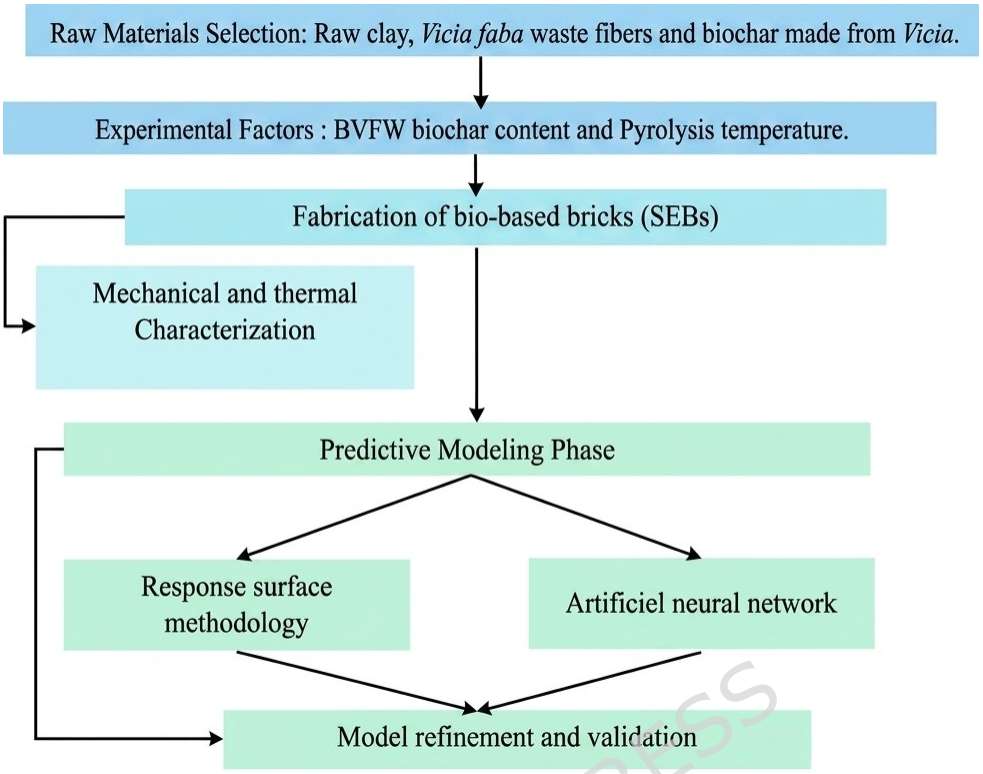

Fig. 4. Methodological framework of adobe bricks reinforced with biochar and *Vicia faba* fibres used in this study.

.

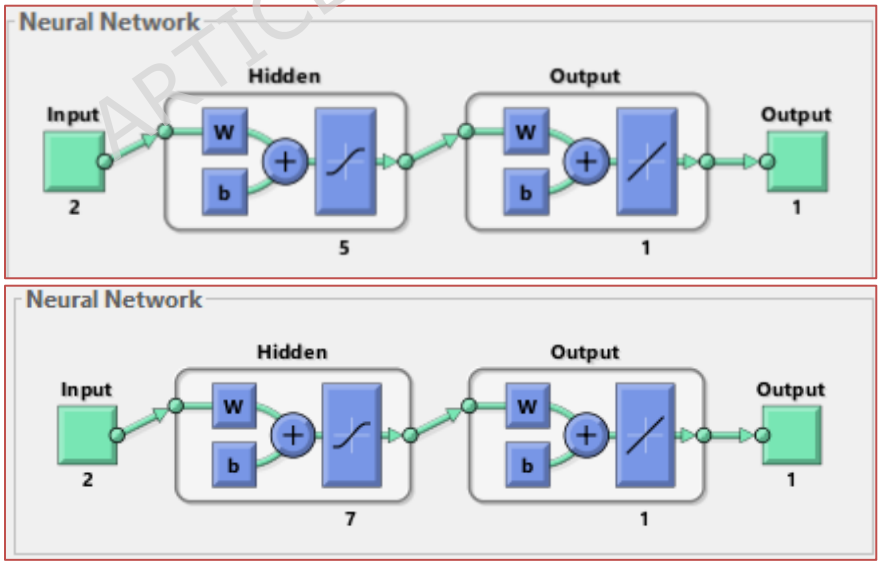

ARTICLE IN PRESS

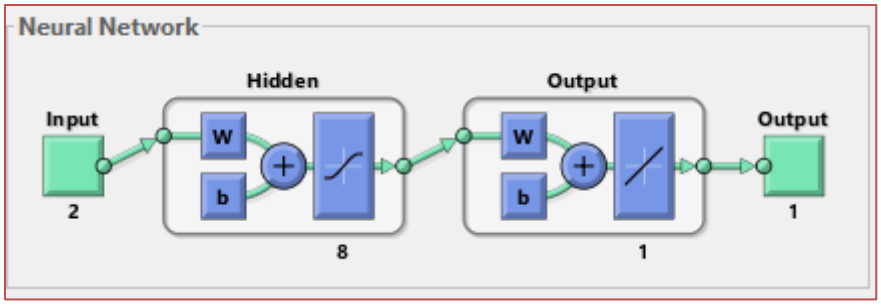

Fig. 5. Architecture of artificial neural networks (ANNs) used in this work of adobe bricks reinforced with biochar and *Vicia faba* fibres.

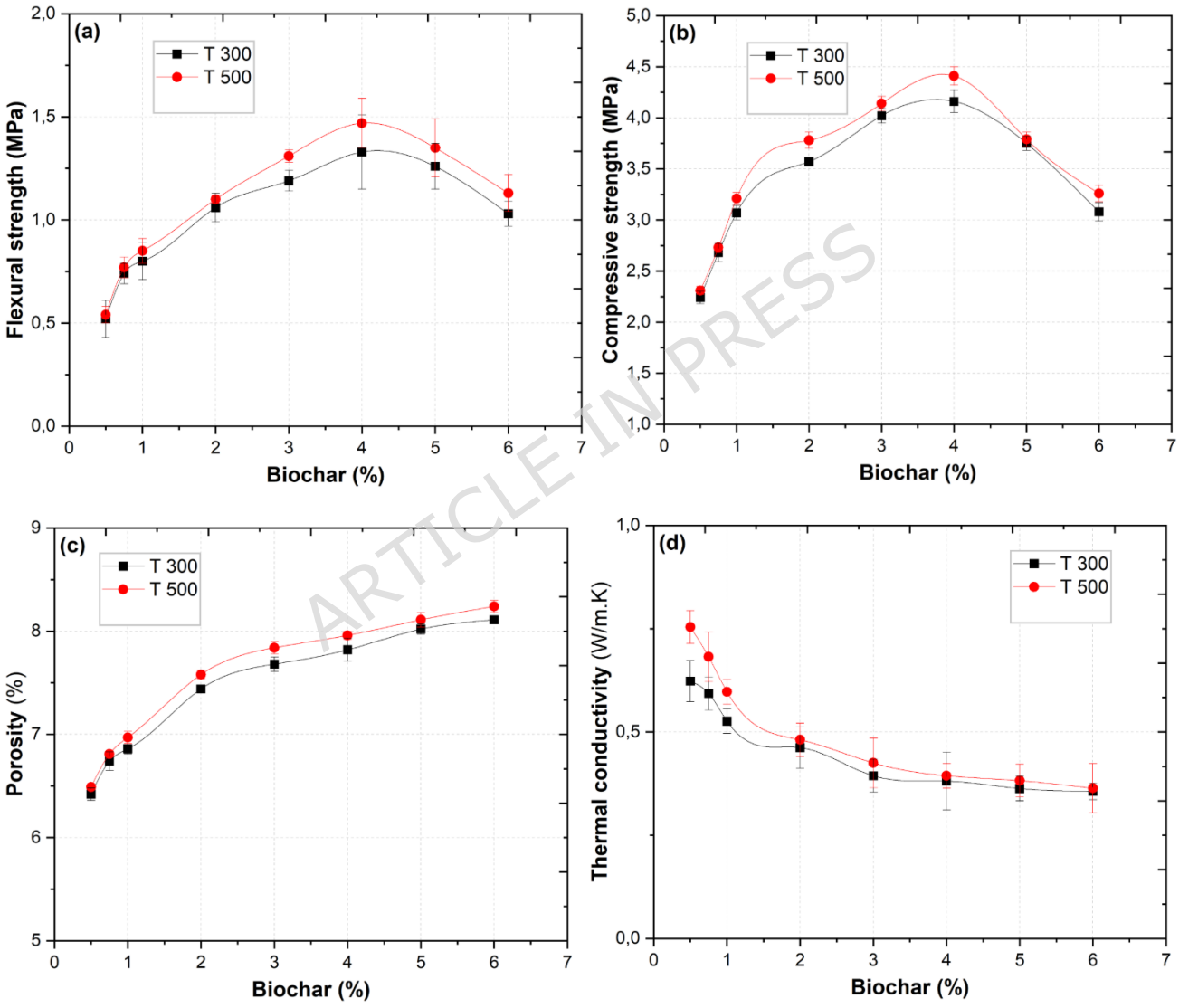

Fig. 6. Flexural strength (FS), compressive strength (CS), porosity, and thermal conductivity (TC) as functions of biochar percentage from *Vicia faba* waste (B*Vf*W) and temperature of adobe bricks reinforced with biochar and *Vicia faba* fibres.

ARTICLE IN PRESS

Fig. 7. Fracture surfaces of adobe bricks reinforced with biochar and *Vicia faba* fibres.

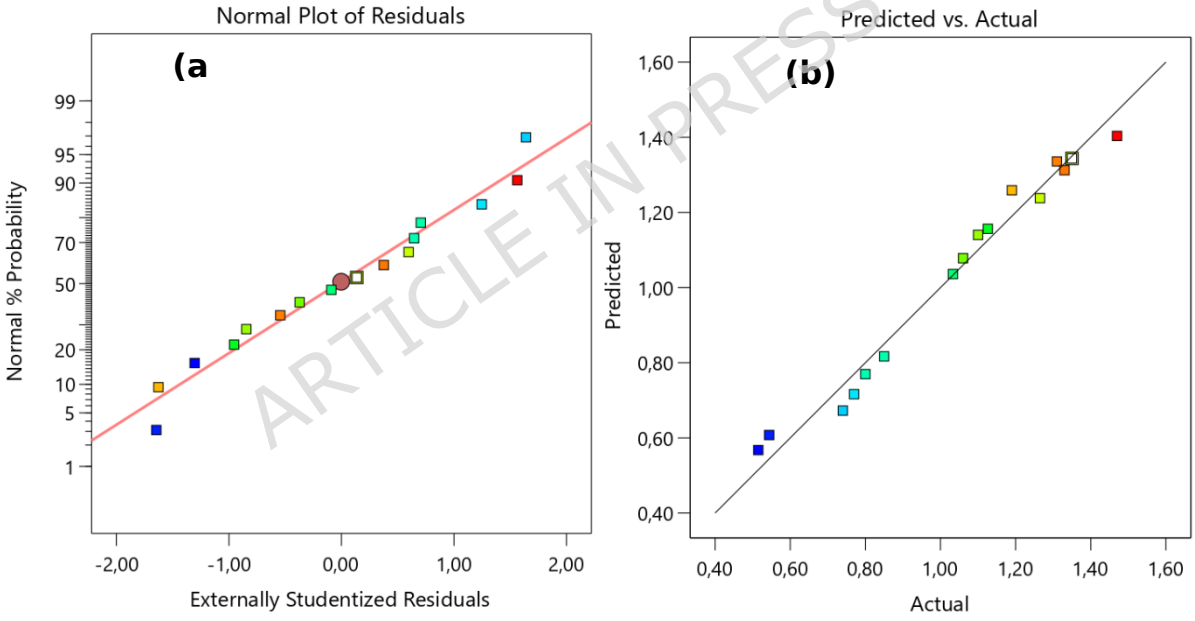

ARTICLE IN PRESS

ARTICLE IN PRESS

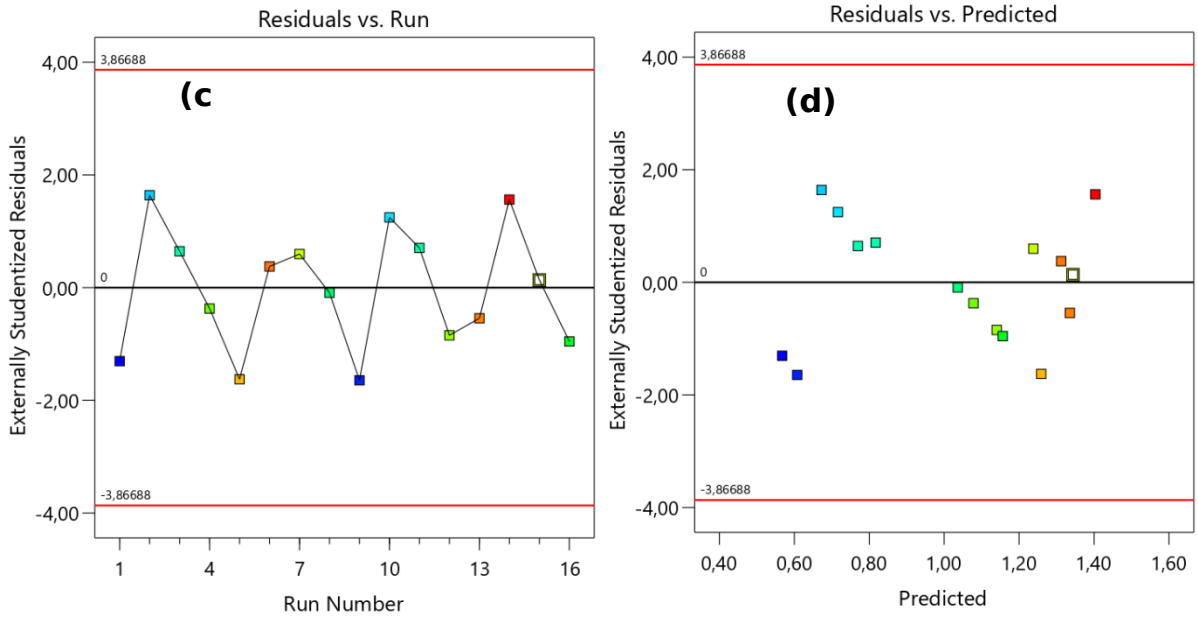

Fig. 8. Diagnosis of the bricks' flexural strength (FS) model; (a) Normal probabilities *vs.* residuals, (b) Predictions *vs.* actual values, (c) Residuals *vs.* the order of realization, and (d) Residuals *vs.* predictions.

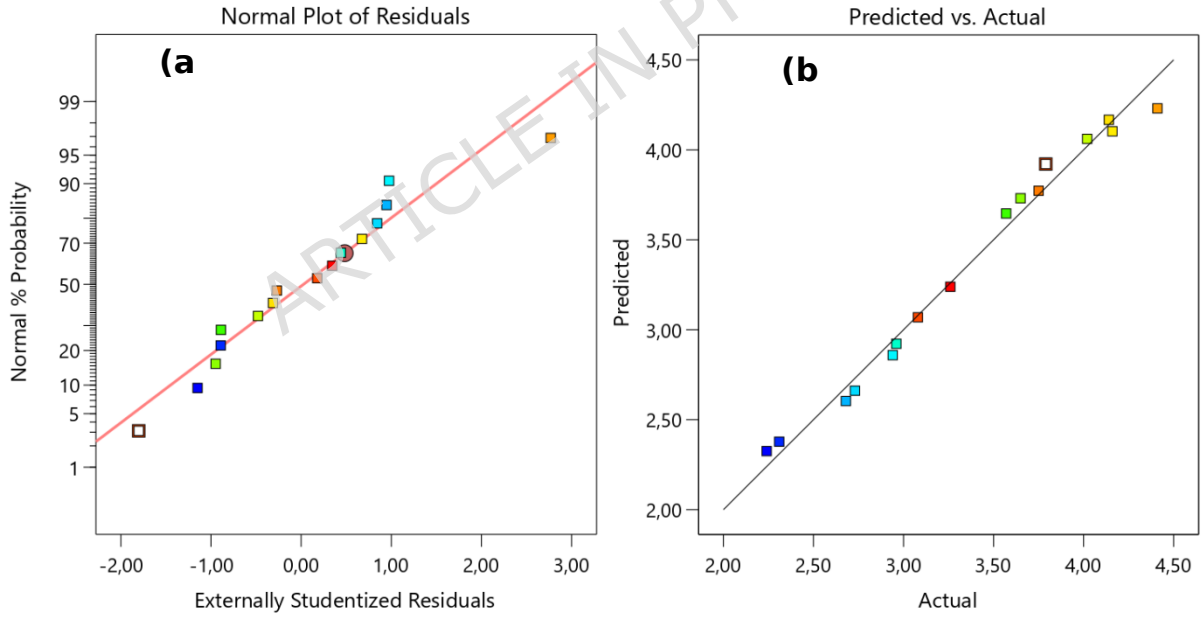

ARTICLE IN PRESS

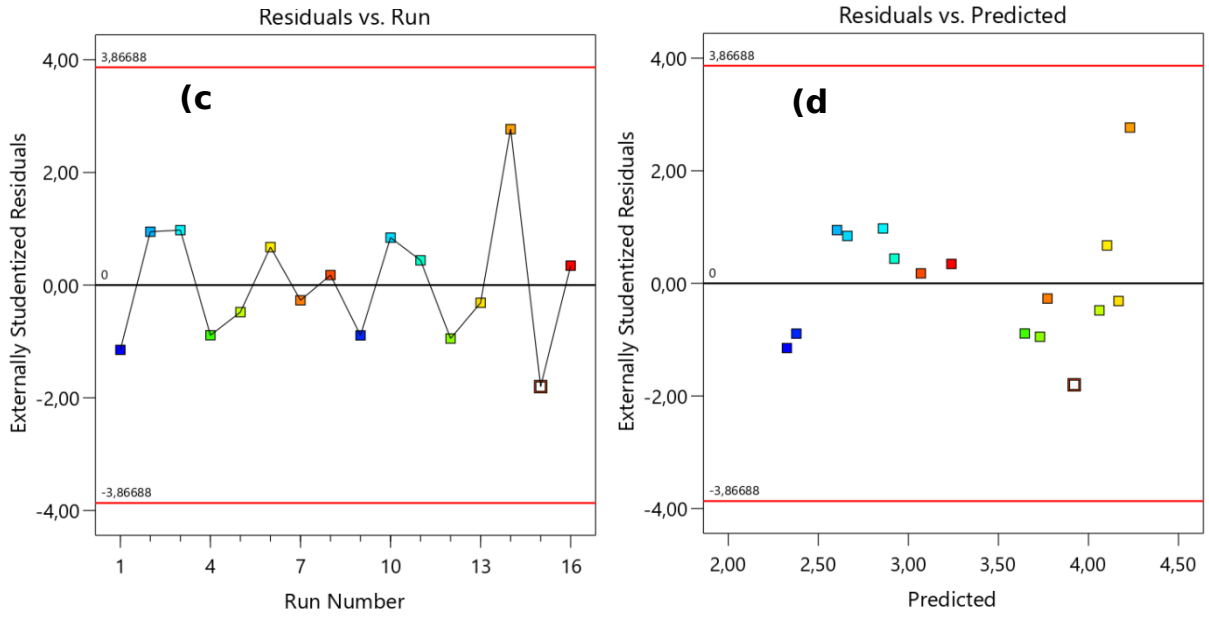

Fig. 9. Diagnosis of the bricks' compressive strength (CS) model; (a) Normal probabilities *vs.* residuals, (b) Predictions *vs.* actuals, (c) Residuals *vs.* the order of realization, and (d) Residuals *vs.* predictions.

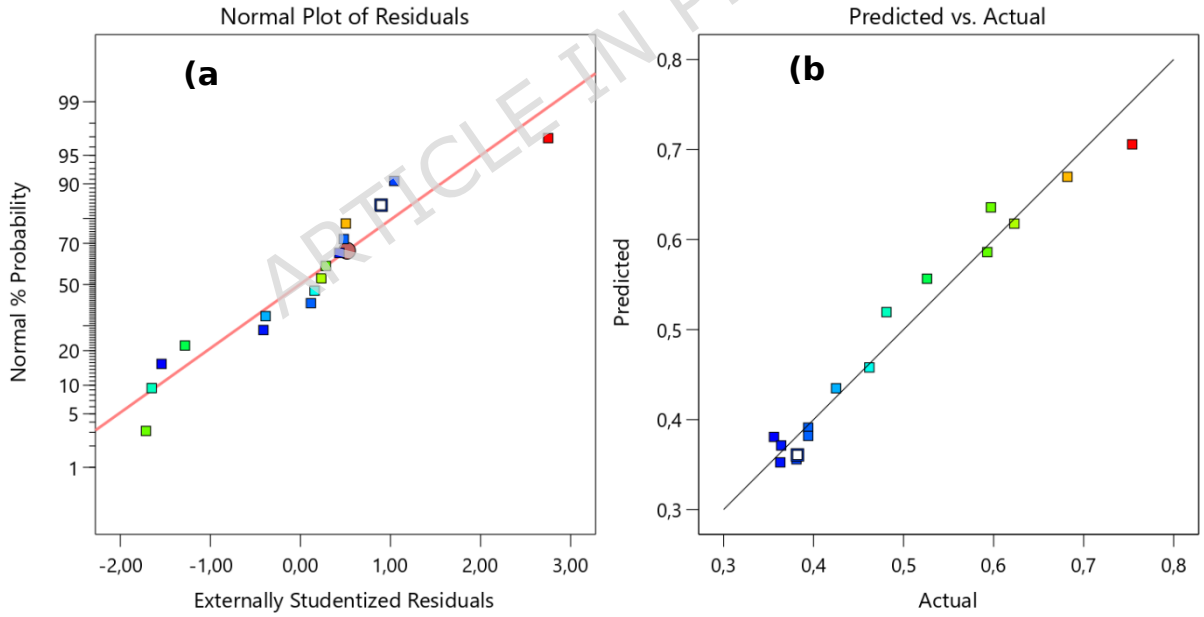

ARTICLE IN PRESS

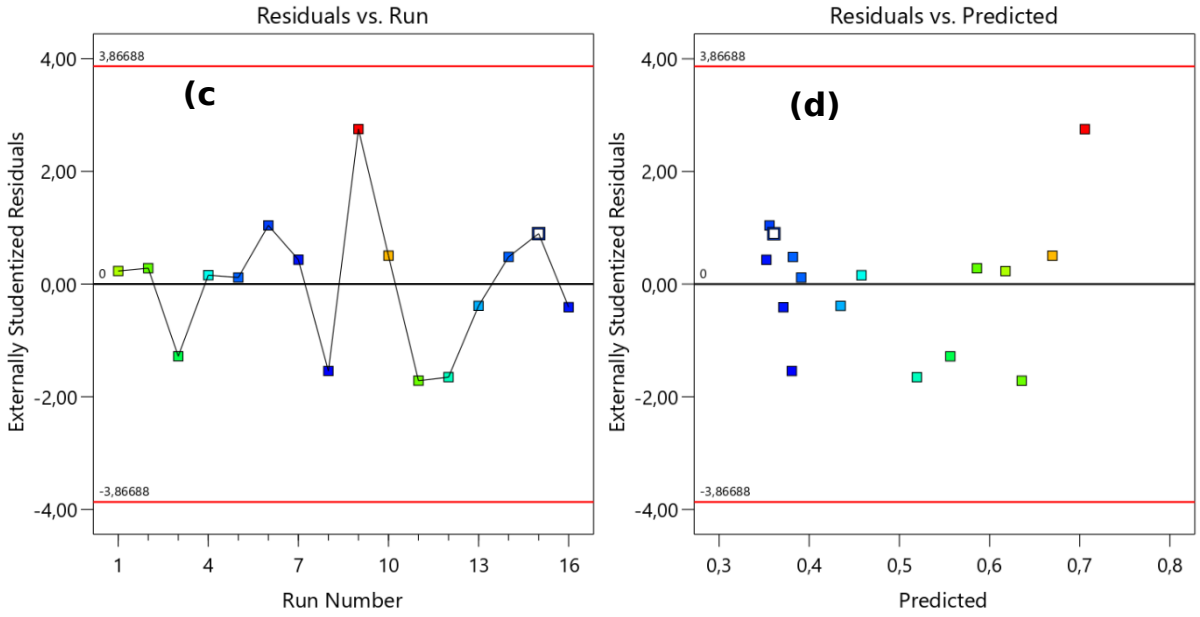

Fig. 10. Diagnosis of the bricks' thermal conductivity (TC) model; (a) Normal probabilities *vs.* residuals, (b) Predictions *vs.* actuals, (c) Residuals *vs.* the order of realization (d), and residuals *vs.* predictions.

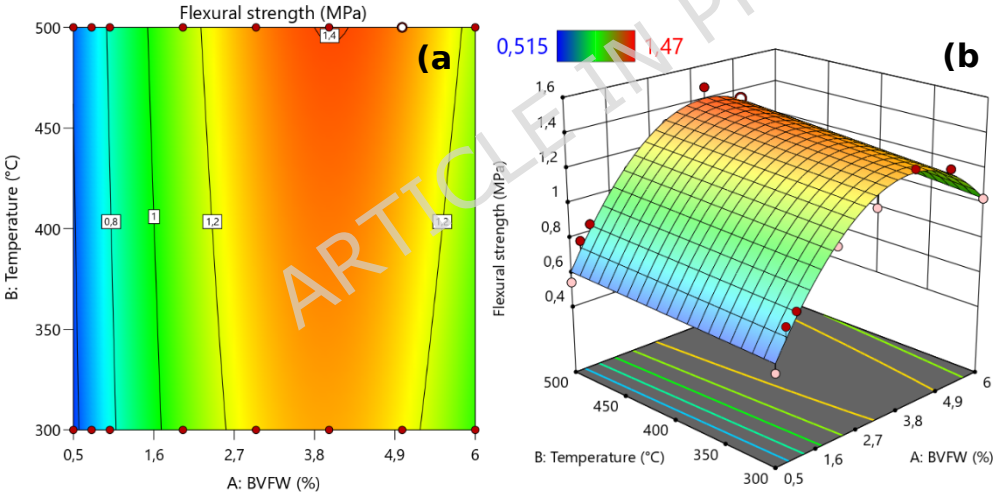

ARTICLE IN PRESS

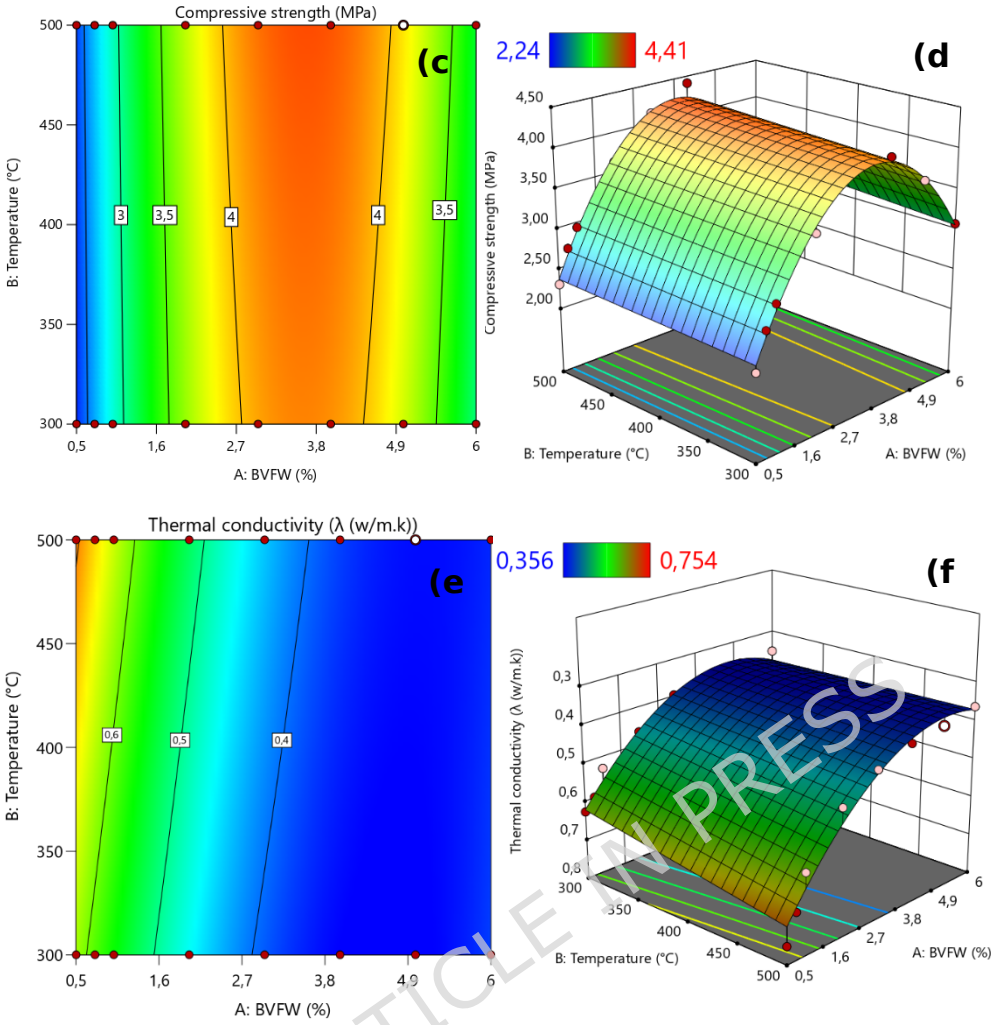

Fig.11. Contour plots and 3D response surfaces: (a, b) flexural strength (FS), (c, d) compressive strength (CS), and (e, f) thermal conductivity (TC) of adobe bricks reinforced with biochar and *Vicia faba* fibres.

.

ARTICLE IN PRESS

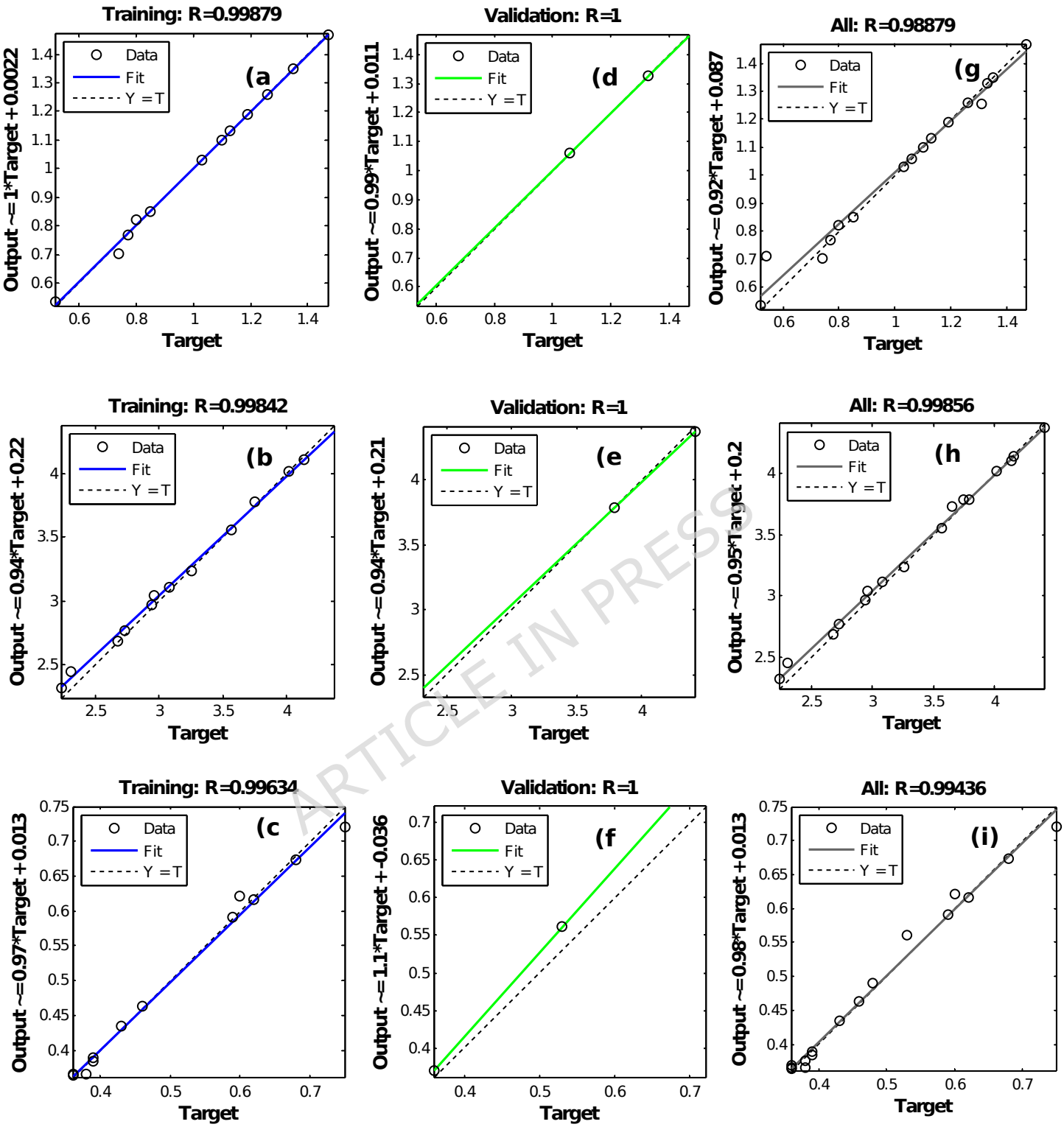

Fig. 12. Actual *vs.* predicted values of Artificial Neural Network (ANN) models for training (a–c), validation (d–f), and the entire dataset: (g-i) for bending strength, compressive strength (CS), and thermal conductivity

ARTICLE IN PRESS

(TC), respectively of adobe bricks reinforced with biochar and *Vicia faba* fibres.

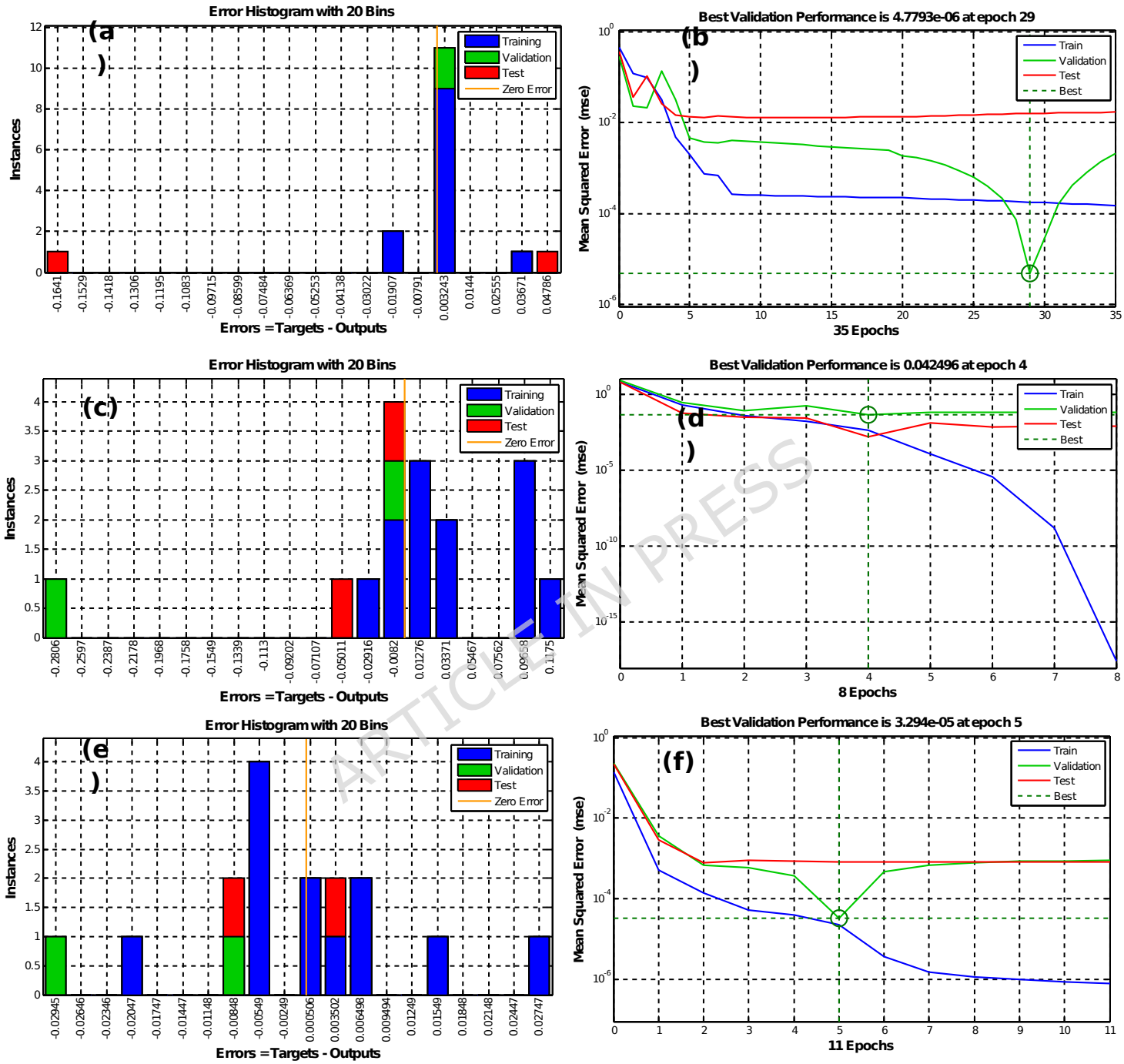

Fig. 13. Fluctuations in deviation histogram over time and mean square error for (a-b) bending strength, (c-d) compressive strength (CS), and (e–f) thermal conductivity (TC), respectively of adobe bricks reinforced with biochar and *Vicia faba* fibres.

ARTICLE IN PRESS

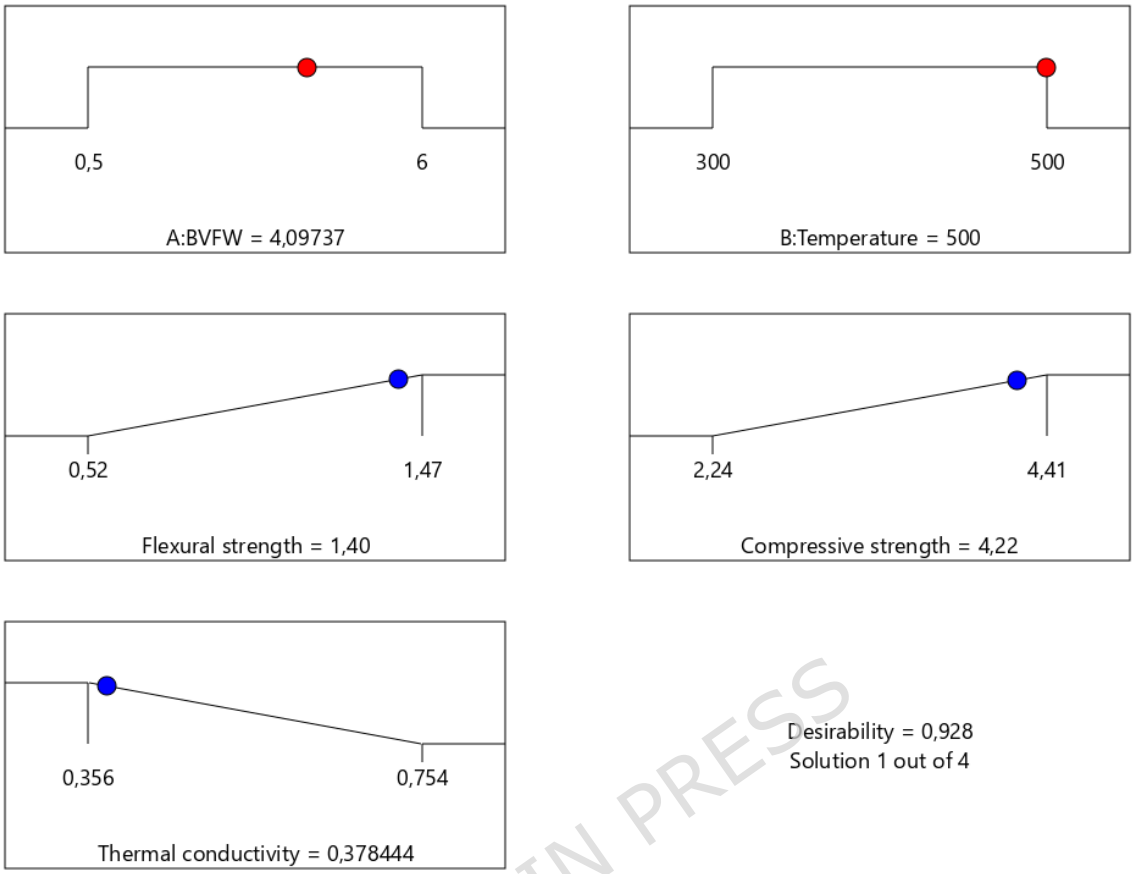

Fig. 14. Optimal responses to compressive stress, flexural stress (FS), and thermal conductivity (TC) based on predicted ramping of adobe bricks reinforced with biochar and *Vicia faba* fibres.

Table 1. Design of various process test parameters and their levels. (B*VfW*: Biochar derived from *Vicia faba* waste).

Factor	Unit	Symbol	Levels		
			Min (-1)	Medium (0)	Max (+1)
B*VfW*	%	A	0.5	3	6
Pyrolysis temperature	°C	B	300	-	500

ARTICLE IN PRESS

Table 2. Bricks' values for thermal conductivity (TC), compressive strength (CS), and bending strength. (FS: Flexural strength, B*VF*W: Biochar derived from *Vicia faba* waste).

Mixture	Factors		Responses		
Run	A- B*VF*W (%)	B- *T* (°C)	FS (MPa)	CS (MPa)	TC (W/m.K)
1	0.5	300	0.52±0.09	2.24±0.06	0.62±0.05
2	0.75	300	0.74±0.05	2.68±0.09	0.59±0.04
3	1	300	0.8±0.09	2.94±0.05	0.53±0.03
4	2	300	1.06±0.07	3.57±0.04	0.46±0.05
5	3	300	1.19±0.05	4.02±0.07	0.39±0.04
6	4	300	1.33±0.18	4.16±0.11	0.38±0.07
7	5	300	1.26±0.11	3.75±0.05	0.36±0.03
8	6	300	1.03±0.06	3.08±0.04	0.36±0.02
9	0.5	500	0.54±0.04	2.31±0.02	0.75±0.04
10	0.75	500	0.77±0.05	2.73±0.03	0.68±0.06
11	1	500	0.85±0.06	2.96±0.06	0.60±0.03
12	2	500	1.1±0.02	3.65±0.04	0.48±0.04
13	3	500	1.31±0.03	4.14±0.06	0.43±0.06
14	4	500	1.47±0.12	4.41±0.04	0.39±0.03
15	*5*	*500*	1.35±0.14	3.79±0.07	0.38±0.04
16	6	500	1.13±0.09	3.26±0.06	0.36±0.06

Table 3. Data on brick flexural, compressive, and thermal conductivity (TC) modeling and experiments. (RSM: Response Surface Methodology, ANN: Artificial Neural Network, FS: Flexural strength, CS: Compressive strength, B*VF*W: Biochar from *Vicia faba* waste, EXP: Experiment).

Runs of	Input variables	Outputs		
		FS (MPa)	CS (MPa)	TC (W/m K)

ARTICLE IN PRESS

experiment	A-BBVfW (%)	B-T (°C)	EXP	ANN	RSM	EXP	ANN	RSM	EXP	ANN	RSM
1	0.5	300	0.52	0.55	0.56	2.24	2.39	2.33	0.62	0.62	0.63
2	0.75	300	0.74	0.69	0.67	2.68	2.66	2.6	0.59	0.58	0.57
3	1	300	0.8	0.8	0.76	2.94	2.89	2.86	0.53	0.53	0.55
4	2	300	1.06	1.07	1.08	3.57	3.62	3.65	0.46	0.45	0.46
5	3	300	1.19	1.2	1.26	4.02	4.06	4.06	0.39	0.39	0.4
6	4	300	1.33	1.27	1.31	4.16	4.06	4.1	0.38	0.37	0.36
7	5	300	1.26	1.26	1.24	3.75	3.62	3.77	0.36	0.36	0.35
8	6	300	1.03	1.03	1.04	3.08	3.02	3.07	0.36	0.36	0.38
9	0.5	500	0.54	0.53	0.60	2.31	2.65	2.38	0.75	0.75	0.71
10	0.75	500	0.77	0.71	0.72	2.73	2.74	2.66	0.68	0.68	0.67
11	1	500	0.85	0.83	0.82	2.96	2.88	2.92	0.6	0.59	0.63
12	2	500	1.1	1.12	1.14	3.65	3.62	3.73	0.48	0.48	0.51
13	3	500	1.31	1.27	1.34	4.14	4.19	4.17	0.43	0.43	0.44
14	4	500	1.47	1.35	1.40	4.41	4.32	4.23	0.39	0.39	0.38
15	5	500	1.35	1.36	1.34	3.79	3.88	3.92	0.38	0.37	0.36
16	6	500	1.13	1.14	1.16	3.26	3.17	3.24	0.36	0.35	0.37

Table 4. Analysis of Variance (ANOVA) for thermal conductivity (TC), flexural strength (FS), and compressive strength (CS). (DF: Desirability function, MS: Mean square, CV: Coefficient of variation, R^2: Correlation coefficient, AP: Adequate precision, SD: Standard deviation, *F*-value: Fisher's F statistic, BVfW: Biochar derived from *Vicia faba* waste).

Source	DF	SS	MS	*F*-value	Prob.	Remark
a) FS						
Model	4	1.27	0.3171	116.11	< 0.0001	Significant
A-BVfW	1	0.4938	0.4938	180.78	< 0.0001	
B-Temp	1	0.0243	0.0243	8.90	0.0124	
AB	1	0.0032	0,0032	1.17	0.3025	
A^2	1	0.5159	0.5159	188.88	< 0.0001	
B^2	0	0.0000		116.11	< 0.0001	
Residual	11	0.0300	0.0027			
Cor Total	15	1.30				
SD = 0.052 Mean = 1.03 CV = 5.08					R^2= 0.9769 R^2 adjusted = 0.9685 R^2 predicted = 0.9505 AP = 28.6106	
b) CS						
Model	4	6.79	1.70	188.84	< 0.0001	Significant

ARTICLE IN PRESS

A-B *VfW*	1	1.23	1.23	136.72	< 0.0001
B-Temp	1	0.0468	0.0468	5.20	0,0435
AB	1	0.0068	0.0068	0.7601	0,4019
A^2	1	4.40	4.40	489.34	< 0.0001
B^2	0	0.0000		14.24	
Residual	11	0.0989	0.0090		
Cor Total	15	6.89			
SD = 0.0948 Mean = 3.35 CV = 2.83					R^2= 0.9856 R^2 adjusted =0.9804 R^2 predicted = 0.9725 AP =35.9346

c) TC

Model	4	0.2358	0.0590	75.56	< 0.0001	Significant
A-B *VfW*	1	0.1558	0.1558	199.68	< 0.0001	
B-Temp	1	0.0058	0.0058	7.49	0,0194	
AB	1	0.0047	0.0047	6.02	0,0320	
A^2	1	0.0318	0.0318	40.82	< 0.0001	
B^2	0	0.0000				
Residual	11	0.0086	0.0008			
Cor Total	15	0,2444				
SD = 0.0279 Mean = 0.4861 CV = 5.75						R^2= 0.9649 R^2 adjusted =0.9521 R^2 predicted = 0.9170 AP =22.6245

ARTICLE IN PRESS

ARTICLE IN PRESS

Table 5. Details on Artificial Neural Network (ANN) data processing. (MSE: Mean Square Error, FS: Flexural strength, CS: Compressive strength, TC: Thermal conductivity, R^2: Correlation coefficient).

Model	Network architecture		Percentage	Samples	*MSE*	R^2
FS	2-5-1	Training	70	12	1.43276E-05	0.9988
		Validation	15	2	4.17483E-04	0.9999
		Testing	15	2	3.24356E-03	0.9896
CS	2-7-1	Training	70	12	2.67832E-06	0.9984
		Validation	15	2	1.42134E-04	0.9999
		Testing	15	2	5.34528E-02	0.9982
TC	2-8-1	Training	70	12	4.65732E-04	0.9963
		Validation	15	2	2.14325E-04	0.9999
		Testing	15	2	6.38912E-05	0.9946

ARTICLE IN PRESS

ARTICLE IN PRESS

Table 6. Predicted values of bricks' thermal conductivity (TC), compressive strength, and bending strength generated by an Artificial Neural Network (ANN).

ANN responses	Mathematical models
Bending_strength	1.0531 × H1 + 0.0260 × H2 - 0.4646 × H3 - 2.4746 × H4 + 0.5095 × H5 + 0.1986 H1 = tanh(.5×(0.4625× BVfW - 0.0005 ×T + 1.3287)) H2 = tanh(.5×(-0.5863× BVfW - 0.0007 ×T + 1.1497)) H3 = tanh(.5×(-0.9982× BVfW + 0.0001 ×T - 1.1437)) H4 = tanh(.5×(0.1901× BVfW - 0.0014 ×T + 0.2591)) H5 = tanh(.5×(-0.0196× BVfW - 0.0044 ×T + 1.4647))
Compressive strength	0.3958 × H1 - 0.5503 × H2 - 0.9177 × H3 - 0.8691 × H4 - 0.2876 × H5 - 0.9713 × H6 + 0.7997 × H7 + 2.8313 H1 = tanh(.5×(-0.1373× BVfW - 0.0119×T + 3.7556)) H2 = tanh(.5×(0.2175× BVfW + 0.0044×T - 1.2570)) H3 = tanh(.5×(0.4365× BVfW - 0.0041×T + 1.1178)) H4 = tanh(.5×(-1.0733× BVfW - 0.0050×T + 0.5429)) H5 = tanh(.5×(0.0381× BVfW + 0.0045×T - 0.7362)) H6 = tanh(.5×(-1.1705× BVfW - 0.0032×T - 0.8913)) H7 = tanh(.5×(-0.3509× BVfW + 0.0003×T + 0.236))
Thermal conductivity	-0.0291 × H1 + - 0.2066 × H2 + - 0.962466 × H3 + - 0.4351 × H4 + 0.0065 × H5 + - 0.0666 × H6 + - 0.3989 × H7 + - 0.2818 × H8 + 0.8503 H1 = tanh(.5×(0.1709× BVfW - 0.0105×T + 4.2692)) H2 = tanh(.5×(0.3436× BVfW + 0.0146×T - 6.9969)) H3 = tanh(.5×(-0.1532× BVfW - 0.0026×T + 1.8027)) H4 = tanh(.5×(0.3285× BVfW + 0.0029×T - 0.7858)) H5 = tanh(.5×(-0.2801× BVfW + 0.0035×T - 0.9641)) H6 = tanh(.5×(-0.7310× BVfW - 0.0046×T - 0.2158)) H7 = tanh(.5×(0.6050× BVfW + 0.0001×T + 1.0053)) H8 = tanh(.5×(-0.4280× BVfW - 0.0031×T + 1.0123))

ARTICLE IN PRESS

ARTICLE IN PRESS

Table 7. Correlation coefficient (R^2), mean square error (MSE), and root mean square error (RMSE) for Flexural Strength (FS), CS, and TC as determined by Response Surface Methodology (RSM) and Artificial Neural Network (ANN).

Responses	R^2		MSE		RMSE	
	RSM	ANN	RSM	ANN	RSM	ANN
FS	0.9769	0.9888	0.3032	0.1043	0.1232	0.1106
CS	0.9856	0.9986	0.4653	0.0213	0.0645	0.0253
TC	0.9649	0.9944	0.4537	0.1165	0.4564	0.0231

Table 8. Goals and variations of optimization variables. (FS: Flexural strength, CS: Compressive strength, B*VfW*: Biochar from *Vicia faba* waste).

Title	Objective	Lower level	Upper level
A: B*VfW* **%**	In range	0.5	6
B: Temperature	In range	300	500
FS	Maximize	0.51	1.47
CS	Maximize	2.24	4.41
TC	Minimize	0.36	0.75

ARTICLE IN PRESS

Table 9. Experimental results and optimization parameters. (RSM: Response Surface Methodology, DF: Desirability Function, ANN: Artificial Neural Network, FS: Flexural Strength, CS: Compressive Strength, B*VfW*: Biochar Derived from *Vicia faba* Waste).

Name	**Input variables**		**Responses**		
	B*VfW* **content (°C)**	**Temperature (%)**	**FS (MPa)**	**CS (MPa)**	**TC (W/K.m)**
Objective	In range	In range	Maximum	Maximum	Minimum
Optimization ANN/GA	4	500	1.44	4.36	0.34

ARTICLE IN PRESS

Optimization RSM/DF	4.09	500	1.40	4.22	0.38
Experimental tests	4	500	1.43	4.32	0.35

ARTICLE IN PRESS